arXiv:astro-ph/9606050v1 8 Jun 1996

Scheduled to appear in the September 1996 issue of The Astronomical Journal

AN HST STUDY OF OB ASSOCIATIONS AND STAR CLUSTERS IN M101 [1]

Fabio Bresolin, Robert C. Kennicutt, Jr.
Steward Observatory, University of Arizona, Tucson, AZ 85721. E-mail: fabio@as.arizona.edu, robk@as.arizona.edu

and

Peter B. Stetson
Dominion Astrophysical Observatory, 5071 West Saanich Road, Victoria, BC, V8X 4M6, Canada.
E-mail: stetson@dao.nrc.ca

ABSTRACT

The massive stellar content, the OB associations and the star clusters in an HST field in M101 = NGC 5457 are investigated. A clustering algorithm yields 79 putative associations. Their size distribution is similar to that found in the Magellanic Clouds, M31 and M33, with an average size around 90 pc. The V luminosity function for the stars contained within the associations has a slope $d\log N/dV = 0.60 \pm 0.05$, while an average reddening E$(B-V) = 0.21$ mag is measured. The stellar content is further discussed by means of color-magnitude and color-color diagrams. Ages are estimated using theoretical isochrones, and range between 3 and 14 Myr ($\pm$2 Myr). We find a suggestion that the upper mass limit of the IMF for stars in OB associations in M101 may be quite high, contrary to some theoretical expectations that the mass limit should be lower in a high metallicity environment. Forty-one star cluster candidates and two H II region core clusters are identified in the M101 field, and their integrated photometric properties are compared with the cluster system of the LMC and M33. Most of the M101 clusters probably belong to the class of young, populous star clusters such as are found in the LMC. Red clusters are rare in this field. In the Appendix the objective finding algorithm is applied to the brightest stars in the Large Magellanic Cloud.

[1] Based on observations with the NASA/ESA *Hubble Space Telescope*, obtained at the Space Telescope Science Institute, which is operated by AURA, Inc., under NASA contract NAS 5-26555

1. INTRODUCTION

OB associations provide valuable information on the physical processes that govern star formation in galaxies. Unlike star clusters, which are gravitationally bound systems consisting of presumably coeval stars, OB associations are loose, short-lived entities, and as such they are natural tracers of recent or current star formation (Blaauw 1991). A better understanding of massive stars has resulted from the investigation of these objects in the Galaxy and in the Magellanic Clouds (Garmany 1994). The study of the spatial distribution of OB associations can provide an insight into the mode of star formation (stochastic vs. density wave triggering), while the size distribution of the associations is directly related to the question of the importance of the associations and star complexes as fundamental building blocks of the structure of spiral galaxies (Efremov and Chernin 1994). On the other hand star clusters hold clues about galactic evolution on longer timescales.

The main advantage of studying OB associations in galaxies other than the Milky Way lies in the possibility of minimizing the difficulties that arise from uncertain distances and high levels of obscuration in the plane of the Galaxy. However we must deal with the long-standing problem of identifying stellar associations in a consistent way for different galaxies. Hodge (1986) pointed out how the measured association properties depend on several selection effects, among these the quality of the observational material and the identification criteria adopted. To overcome this problem *automated* identification techniques have been recently applied to nearby, resolved galaxies. In this work, which introduces a project aimed at defining some of the properties of OB associations and star clusters in different galactic environments (metallicity, star forming activity, etc.), we present the results obtained for M101 with a similar objective technique, and describe the methodology adopted for investigating associations and clusters in external galaxies. Our goal is to analyze galaxies of different Hubble types and distances (up to 15 Mpc with HST), in order to compare their OB associations, their star clusters, and their massive stellar content. This can provide clues on the possible variations of stellar populations and massive star formation among galaxies.

We present the observational material and the data reduction in § 2. Results on the massive stars are discussed in § 3. The identification technique and the size distribution of the OB associations in M101 are discussed in § 4 and § 5, respectively. In § 6 we analyze the properties of the stellar content of the associations. In § 7 we draw some tentative conclusions on the stellar IMF in the field studied. The results on star clusters are presented in § 8. In the Appendix we apply the objective algorithm to the LMC. A distance to M101 of 7.4 Mpc (Kelson *et al.* 1996) is adopted.

2. OBSERVATIONS AND DATA REDUCTION

The HST Distance Scale Key Project is observing 18 galaxies to detect Cepheid variables (Kennicutt, Freedman and Mould 1995). As a by-product of this effort, a large number of WFPC2 images of spiral galaxies is produced, suitable for the study of their stellar populations. Figure 1 shows the inner field of M101 = NGC 5457 studied in this work (see also Stetson *et al.* 1996). The apex of the four chips lies at $\alpha = 14^{\rm h}03^{\rm m}24\overset{\rm s}{.}0$ and $\delta = 54°21'38''$ (2000.0), $1\overset{'}{.}8$ NE of the center of M101, as shown in Fig. 2. The filters used for the observations were F336W (two 1200s exposures), F439W (two exposures, 1000s and 1200s respectively), F555W (12 1200s exposures) and F814W (one 1000s and four 1200s exposures). The stellar photometry was carried out with the multiple-frame profile-fitting package ALLFRAME (Stetson 1994). In order to create a master list of stellar objects, a median image of each chip, free of cosmic rays, was generated from all the available single-epoch images. Once the stellar list was made using the PSF-fitting program ALLSTAR, we performed the photometry for each of the single-epoch images with ALLFRAME. The average magnitudes were calibrated and transformed to the *UBVI* system with the equations and zero points of Holtzman *et al.* (1995). For the following analysis only stars that were measured in all four filters were retained, giving a total of 16812 stars.

Table 1 lists the typical photometric errors at various magnitudes. The exposure times for the B and U frames were not long enough to accurately measure stars fainter than $V{\sim}24$. This imposes some limitations on the analysis of the fainter stars, but not on the brighter ones which are of interest here. The incompleteness in the V photometry was estimated by reducing copies of the V frames of chip 4 (the most crowded) to which 1,000 artificial stars were added. Virtually all stars down to $V{=}\,25$ were recovered, 93% at $V{=}\,25.5$, 80% at $V{=}\,26$. However, in our study of the luminosity function (§ 6.1), incompleteness is seen to set in at $V{\sim}23.5$ and appears to be more severe than stated above at fainter magnitudes. Since only stars recovered in all four filters were included, this can be ascribed to two causes: shorter exposure times in B and U, and the fact that the artificial stars were added at completely random places within the field, whereas the majority of real stars are – by definition – located in regions of higher-than-average stellar density, and are therefore more subject to crowding and confusion. Approximate completeness limits, without restriction to stars detected in all four filters, are $V{\sim}23.5$ in U and B and $V{\sim}25$ in V and I.

Ground-based images at Hα and Hβ of a region partly overlapping with the HST field were secured in March 1994 with the Steward Observatory 90-inch telescope on Kitt Peak. These data are used in § 6.2 to independently estimate the reddening in the corresponding OB associations.

3. MASSIVE STARS

Figure 3 shows the color-magnitude diagram (CMD) for ∼16,000 stars recovered in the field studied. The evolutionary tracks, taken from Schaller *et al.* (1992), were converted to the observational plane using the equations of Massey *et al.* (1995a). They were reddened by

E$(B-V) = 0.21$, corresponding to the mean extinction measured for the stars. This diagram shows that we are detecting stars typically above 10 $M_\odot$. The width of the blue plume is ∼0.5 magnitudes for V<24.5, and increases to one magnitude at the faint end. This is much larger than what is observed in OB associations in the LMC (Massey *et al.* 1989, Hunter *et al.* 1995). The stellar models of Schaller *et al.* (1992) predict a wide main sequence for the H-R diagram of massive stars. However, given the photometric uncertainties (Table 1), the observed scatter is largely explained by photometric errors alone, and perhaps partially by an age spread among non-coeval populations of stars and by differential reddening. Similar conclusions were drawn by Hunter and Thronson (1995) for HST data of I Zw 18. Effects of blending are surely present, as many stars are located in crowded regions, so that several of the brightest objects could in fact be groups rather than single stars. To reduce this effect for the brightest objects, we have removed from the CMD all stars brighter than $V = 22$ that do not appear to be isolated stars. The result is shown in the inset of Fig. 3, where the photometric errors for each star are indicated.

4. IDENTIFICATION OF OB ASSOCIATIONS

Recently the question of comparing the clustering properties of massive stars in different galaxies has been attacked by adopting automated algorithms, to remove much of the subjectivity which was intrinsic to previous methods. Wilson (1991) introduced a friends-of-friends algorithm to define groups of bright blue stars in M33. In this method all blue stars lying within a predetermined search radius from another star were included in the same stellar group. The latter was defined as an OB association if it contained at least 10 blue stars. The search radius was determined by the mean surface density of blue stars. A somewhat different method, introduced by Battinelli (1991), determines the search radius that maximizes the number of stellar groups containing a minimum of three stars. The same method has been used by Magnier *et al.* (1993) to identify OB associations in M31.

In this study of M101 we adopted Battinelli's (1991) approach, because of its high level of objectivity and in order to compare association properties of galaxies already studied. The criteria $V< 24.5$ ($M_V < -4.8$) and $(B-V) < 0.4$ (before correcting for reddening) were used to select the blue stars. The search algorithm was applied separately to the four WFPC2 chips because of the gradient in stellar density across the HST field. This gave search radii of $2\farcs4$ (40 pc), $3\farcs5$ (58 pc), $3\farcs9$ (64 pc) and $2\farcs2$ (36 pc) in chips 1, 2, 3 and 4, respectively. These values are very close (to within ± 0.2 arcsec) to what one obtains using Wilson's (1991) definition of search radius based on the stellar surface density. We must stress that the 'associations' defined by the algorithm lie within a two-dimensional projection through a patch of galactic disk or a spiral-arm fragment, and do not *necessarily* lie physically close together in three dimensions, share common space motions, or originate in a single coherent star-forming event; thus we cannot be certain that any given one of them is a true OB association as we would define it in our Milky Way Galaxy. Nevertheless, even though we cannot be sure that these asterisms are genuine, physical OB associations, we can

at least be confident that they represent objectively defined, localized regions of enhanced surface density in the distribution of young, massive stars.

We can perform a statistical test to ascertain how many of the groups found are likely to be chance coincidences. We applied the algorithm to a set of random distributions of stars, each containing the same number of blue stars as the actual data. The search radius was set equal to the value used for the actual data. The simulations showed that the contamination of false associations was less than 10% when the threshold population was set to seven stars or more. We adopted this criterion, which resulted in a total sample of 79 associations, as shown in Figure 4. Fifty contain at least 10 blue stars. The average number of blue stars in the associations is 15 (19 for $N_{blue} \geq 10$). It is likely that the actual number of member stars is larger than these figures, given the possibility of measuring very compact groups of a few stars as a single star. The simulations described do not take into account the fact that young stars are not distributed exactly at random due to the existence of spiral arms and dust lanes.

Our sample is biased against associations that contain very few stars. A major concern is therefore the completeness in the rate of detection of associations. To estimate the incompleteness we made a comparison with the system of associations in the LMC. The area covered by our HST field is approximately equal to the area surveyed by Lucke and Hodge (1970) in the LMC, where 122 associations were catalogued. Correcting for inclination effects and scaling to the number of LMC associations, we should have detected ∼100 associations in the M101 field. We might therefore be incomplete by 20%, on the assumption that the two galaxies are directly comparable. Appendix A shows however that when the objective algorithm is applied to the LMC, the same number of associations is detected as were found in the works of Lucke and Hodge (1970). A possible cause for incompleteness arises from the difficulty in establishing very small groups of blue stars as real associations. Our search method regards most of the smallest groups as statistically insignificant, but many of them could be very compact associations, for which we are not sensitive enough. This means that we are not detecting "Orion-like" objects in M101. Instead the smallest objects in our sample correspond to Galactic star forming regions with size between that of M8 and the Rosette Nebula (NGC 2244), both in terms of diameter and Hα luminosity (Kennicutt 1984). At the high-end we find Galactic counterparts in the Carina and W49 regions, while the most luminous association (# 72) has an Hα luminosity comparable to 30 Doradus in the LMC. On the other hand we think that our search method is conservative, in the sense of disregarding associations of dubious reality, which will be very important when studying galaxies at even larger distances. We are therefore at a necessary trade-off between completeness and reproducibility.

Since we are interested in comparing results for different galaxies in the future, we ran a simple experiment to test how resolution might affect the identification of the associations. New versions of chip 4 images were created, compressed by a factor of 1.5 and 2, to simulate a corresponding increase in distance (the exposure times were assumed increased by a factor of 2.25 and 4.0 respectively). The search radii were reduced by exactly the same factors with respect to the original images. The average size of the clumps did not change significantly in the first case,

and increased by 10% in the case corresponding to a doubling of the distance. In both cases, most of the original morphology and position of the associations were recovered, while the number of blue stars was reduced by 9% and 19%. These results suggest that we can confidently compare properties of associations in galaxies which differ by at least a factor of two in distance.

5. SIZE DISTRIBUTION OF THE OB ASSOCIATIONS

The diameters of the associations found in M101 are given in Table 3, while Figure 5 compares the size distribution of the M101 associations with other nearby galaxies studied with similar methods. These are the LMC (Appendix), M33 (Wilson 1991 and Regan and Wilson 1993), M31 (Haiman *et al.* 1994), the SMC (Battinelli 1991), and NGC 6822 (Wilson 1992). Somewhat different criteria have been used to select the blue stars in these works; our criterion is equivalent to that applied to M33. We note that the size distributions are dependent on the search radius chosen. All galaxies show a similar distribution, and the Kolgomorov–Smirnov test indicates that the data are indeed consistent with a single distribution function. The presence of a peak might at first be attributed to a selection effect, due to the fact that smaller associations are more difficult to detect. However, an absence of associations smaller than 20-30 pc is observed in even well resolved galaxies such as the Magellanic Clouds (Hodge and Lucke 1970, Hodge 1985), indicating that the observed distributions are indeed peaked. Furthermore in the Galaxy OB associations have a mean size around 140 pc (Garmany and Stencel 1992), much larger than the typical diameters of open clusters (10–35 pc, Janes *et al.* 1988). The peak in the distributions lies around 40–80 pc for M101, LMC, SMC, M33 and NGC 6822, but ∼110 pc for M31. This hint of a possible Hubble-type dependence deserves further investigation. However, it should be noted that the size distribution that Efremov *et al.* (1987) obtained for the M31 associations shows a behavior more closely resembling that of the remaining galaxies.

We believe the size distribution to be more meaningful than the mean diameter, which is difficult to define and is subject to numerous observational biases (see discussion in Magnier *et al.* 1993). We have however compiled in Table 4 the mean for the galaxies studied, which show similar values of ∼90 pc. We conclude that the associations in M101, LMC, SMC, M33, NGC 6822 and perhaps M31 have similar size distributions and average sizes. No clear effect of Hubble type or distance (resolution) is observed.

6. PROPERTIES OF THE OB ASSOCIATIONS

6.1. The stellar luminosity function

Many studies of extragalactic stellar populations use the differential luminosity function (dLF) to investigate possible differences in the properties of the most massive stars (Freedman

1985, Blaha and Humphreys 1989). We have determined the LF in V for all stars contained in the 79 associations, as well as for all stars in our frames, regardless of their position, and for field stars only. We followed Freedman (1985) and Berkhuijsen and Humphreys (1989) in using different color selection criteria to better isolate the blue stars. It was pointed out by Freedman (1985) that a $U-V$ criterion is to be preferred over $B-V$ because the former is a better discriminator against A supergiant stars. Adopting the usual power-law expression for the LF we then determined the slope $\alpha = d\log N/dV$ for different color cut-offs, as given by a least-square fit and using 0.5 mag interval bins. The color criterion that provides the largest slope is the adopted one. Fig. 6 shows the LF in V for stars with $U-V \leq -0.5$. The break in the function for $V>23.5$ suggests that the data become incomplete at that magnitude, and hence we only include stars with $V<23.5$ in our fit. Table 2 lists the best fitted power-law slopes for various color criteria, for the entire field population and stars in associations only. The errors listed include statistical uncertainties but not systematic effects due to crowding or incompleteness. There is no important difference among the three color criteria. The slightly smaller value from the $B-V$ selection is hardly significant, and, if real, might be due to the inclusion of some later-type stars. It is interesting however that no difference is seen between stars in associations and stars in the field. We conclude that the slope of the V LF in this field is $\sim 0.60 \pm 0.05$.

Freedman (1985) found a value of 0.67 ± 0.03 for the V LF of the brightest stars in nearby galaxies. More recent determinations from HST observations are given, among others, by Hughes *et al.* (1994) and Hunter and Thronson (1995). The values found (0.56–0.58 in the case of M81, and between 0.58 and 0.65 for different sets of stars in I Zw 18) are consistent with the slope determined for M101, and confirm that the upper LF does not change significantly. This is perhaps not surprising given the relative insensitivity of the LF slope to changes in the IMF (Massey 1985). However these results appear to rule out any radical variation in IMF slope or stellar mass limit (see § 7).

6.2. Reddening

The substantial extinction in this M101 field is readily inferred from the optical images, which show many dust filaments along the spiral arms, and by the color ($B-V \simeq 0$) of the blue plume in the CMD of Fig. 3. Hence it is important to measure the reddening of the OB associations. The extinction law in M101 was found to be similar to the Galactic one ($R_V = 3.16$, $R_V = A_V/E(B-V)$) by Rosa and Benvenuti (1994). The foreground extinction in the direction of M101 is virtually zero (de Vaucouleurs *et al.* 1991).

To measure the reddenning we used the Johnson Q parameter technique, where $Q = (U-B)-0.72\,(B-V)$ is a reddening-free quantity. The Q value for stars in associations with $B-V< 0.1$ was used to derive, by means of the equations given in Massey *et al.* (1995a), an intrinsic color, $(B-V)_0$, which allowed individual stellar reddenings to be calculated. The mean value for all stars belonging to the same association was then adopted as the reddening for the

entire group. The estimated uncertainty is E($B-V$) = ±0.1. For the stars in our associations the average <E($B-V$)> = 0.21. Wilson (1991) gives an average of 0.3 mag for associations in the inner region of M33 (0.15 in an outer region studied by Regan and Wilson 1993), and values in the range 0.2−0.4 are reported, for example, by Haiman *et al.* (1994).

The ground-based narrow-band imaging was used to measure the extinction for a number of H II regions, some of which match the position of an OB association. The reddening can be measured by the Balmer decrement:

$$\frac{\mathrm{I_{H\alpha}}}{\mathrm{I_{H\beta}}} = \frac{\mathrm{F_{H\alpha}}}{\mathrm{F_{H\beta}}} 10^{\mathrm{C(H\beta)}\cdot f(\lambda)}$$

where we assume the theoretical value $\mathrm{I_{H\alpha}/I_{H\beta}} = 2.86$ (case B, T=10^4 K, N_e=100 cm^{-3}, Osterbrock 1989) and the extinction curve $f\,(\lambda)$ of Seaton (1979). The visual extinction is given as $\mathrm{A}_V = 2.15\cdot\mathrm{C(H\beta)}$ (Rosa and Benvenuti 1994). The average reddening for 35 H II regions is 0.39 mag, with a large scatter (0.19 mag). Of these, 13 coincide with OB associations (nearly 40 percent of the associations have H II region counterparts, but these are often too faint to be included in the analysis). The comparison with the values from the broad-band photometry is shown in Figure 7. The Balmer ratio gives, on average, a reddening value ∼0.1 mag larger than the Q method. This is of the same order as the uncertainties, therefore the difference in the two distributions is to be considered marginally significant. Note also that many of the larger reddening values are found for H II regions that have no OB association counterpart. We could say that the identified OB associations do not lie in the regions with the higher reddening. With such a small sample, though, it is difficult to assert the reality of this effect. In general we expect however that H II regions will be more reddened than the average OB association.

6.3. The color-magnitude and color-color diagrams

We show in Figure 8 the CMD of those stars that lie within the OB associations boundaries. For each association the stars have been dereddened according to the average E($B-V$). The CMD morphology is similar to that of Figure 3, and shows that the selected OB association boundaries contain several evolved stars. The scatter of stars across the diagram can be therefore attributed partly to a spread in age. The age analysis (next section) tends to confirm the presence of stellar groups older than 10 Myr among the selected associations.

The dereddened color-color plot of stars in associations with photometric uncertainties <0.15 mag is shown in Figure 9. The sequences for dwarf and supergiant stars have been drawn, adopting the calibrations of Fitzpatrick and Garmany (1990) and FitzGerald (1970). O–B5 stars ($U-V \leq -0.9$) are clumped around the tip of the sequences. A few B5–B9 and A stars are also present at redder colors. According to the calibration of Fitzpatrick and Garmany (1990) stars of luminosity class Ib have $\mathrm{M}_V \simeq -5.2$ (−4.3) at $U-V \sim -0.9$ (−0.4) (Ia supergiants are at least one magnitude brighter), corresponding to $V \simeq 24$ (25). At this magnitude both B and U frames

are severely incomplete, thus explaining the rapid decline in the number of stars visible below the $U-V = -0.9$ line.

6.4. Estimating the age

We attempted to estimate the age of the OB associations in M101 by comparing their dereddened CMDs by visual comparison with theoretical isochrones (Schaller *et al.* 1992, Meynet *et al.* 1993). Usually the brightest stars were used in the comparison, since the fainter ones tend to have large photometric errors. The major sources of uncertainty in assigning these ages are the reddening, the small number of stars available in individual associations and photometric errors. The presence of binary stars and unresolved clumps is a further problem. An uncertainty of ± 2 Myr is estimated, based on the fact that typical photometric and reddening errors can produce a variation of a few (~ 2) Myr in the calculated ages.

Fig. 10(a) shows an example of this procedure. The isochrones, calculated from 2.5 to 9.5 Myr in steps of 1 Myr, are superposed on the CMD of association # 37. In this case an age of 4 ± 2 Myr was estimated. The evolved stars in the red part of the diagram probably do not belong to the same episode of star formation that created the younger stars. The coexistence of red supergiants and younger OB stars, pointing to non-coevality, has been noted in previous studies (Doom *et al.* 1985, Massey *et al.* 1989, Garmany and Stencel 1992). If the observed red stars are indeed members of the associations, it would mean that star formation occurs in episodes separated by several Myr, and that no single age can be assigned. At least qualitatively, though, there is no apparent clumping of the red stars within the associations boundaries. We conclude that they could appear to belong to the associations simply because of projection effects.

We show in the other panels of Fig. 10 the dependence on age of three quantities: the number of blue stars, the size of the associations and the number of ionizing photons Q_0 (calculated from the Hα flux) for the H II regions which have been identified also as OB associations. The estimated uncertainty of ± 2 Myr is represented by bars elongated along the time axis. Despite the scatter, this shows how the richest and largest associations are found among the youngest ones. This is probably due to the disruption of the gravitationally unbound associations with time, combined with selection effects, which make it easier to detect stars belonging to young associations. There is also a dependence of Q_0 on age, due to the relation between the number of blue, ionizing stars and age. This plot is consistent with the typical H II region lifetime of 5–6 Myr. Table 3 summarizes the associations properties presented in this section.

7. ON THE UPPER MASS LIMIT OF THE IMF

The use of broad-band photometry to study the IMF of distant populations of stars is subject to several difficulties. First of all is the well-known insensitivity of broad-band colors to

the effective temperature of hot, massive stars (Massey *et al.* 1995a). This makes the task of discriminating stars of different masses practically impossible with photometry alone. Moreover incompleteness in the data hinders the detection of the hottest stars, whose large bolometric corrections make them visually fainter than supergiants of later type. Photometric uncertainties and reddening, together with crowding and blending of unresolved stellar images (particularly in the young clusters within the star-forming regions) complicate matters further. With these caveats in mind, we can look at the CMDs of Fig. 3 and 8. These suggest the presence of stars more massive than 25–30 $M_\odot$, perhaps 60 $M_\odot$ or higher. The degeneracy of massive stars in this region of the CMD, though, makes it impossible to say whether very massive stars are unambiguously present or not.

We also attempted to use an evolutionary synthesis model to constrain the upper mass limit of the IMF. Integrated magnitudes and colors for the richest associations (those having more than 15 stars) were measured by adding up all the flux within the association boundaries. The reddening-corrected colors were compared with the models of Leitherer and Heckman (1995) (instantaneous burst, solar metallicity). In Fig. 11 the model predictions for two upper mass limits, 30 and 100 $M_\odot$, of a power-law IMF with Salpeter's slope are superposed on the observed colors and ages. While the comparison for $(U-B)_0$ favors an upper mass limit of 100 $M_\odot$, the other two colors are however more difficult to interpret.

We conclude from this two exercises that there is some evidence for an IMF in M101 with a high cut-off mass (comparable to the $\sim$100 $M_\odot$ limit found in the Magellanic Clouds and in the Milky Way by Massey *et al.* 1995b). This field has an oxygen abundance of $\sim$1–2 $Z_\odot$ (Kennicutt and Garnett 1996) and some authors have suggested previously that the H II regions in this part of M101 have a much lower upper stellar mass limit (*e.g.* Shields and Tinsley 1976). Our observations suggest that such a strong change in the upper mass limit may not be present, but further observation are needed to make a definitive test. This result also agrees with the study of Rosa and Benvenuti (1994), who found no need to invoke a metallicity effect on the IMF in their study of four giant H II regions in M101.

8. POPULOUS STAR CLUSTERS

The importance of star clusters for the understanding of star formation and evolution has been stressed many times (van den Bergh 1991). The clusters of the Magellanic Clouds in particular have been the subject of intense study, leading to a picture of differing evolutionary histories between the Clouds and the Galaxy. Of great interest is the presence in the Clouds of populous clusters ("blue globulars"), which are absent in the Milky Way. Populous clusters have been observed in a handful of galaxies, and Kennicutt and Chu (1988) suggested a Hubble type dependence, being these clusters preferentially found in late-type (Sc, Irr) galaxies. It is therefore interesting to extend the search for populous clusters to as many galaxies as possible. This could lead to a better understanding of the properties and systematics of star formation in galaxies.

Observations with HST like those used in the present work are well suited for this search. With typical sizes larger than 10 pc in the LMC (van den Bergh 1991), we expect to be able to identify these objects at least to a distance of 10-12 Mpc on WFPC2 images.

A total of 41 clusters were found by visual search in the WFPC images, with typical FWHM= 0.″3. Their luminosity was measured with aperture photometry on average images. The estimated uncertainty in the colors is 0.1 magnitudes, based on the variation in the measured fluxes using different apertures and sky annuli. The magnitudes are more uncertain: aperture radii of eight pixels (= 29 pc in the three Wide Field chips) were adopted, but in some cases smaller values had to be used to avoid contamination from nearby objects. The results are summarized in Table 6, while Fig. 12 and 13 show the integrated color-magnitude and color-color diagrams, respectively.

Most clusters are blue ($B-V<0.5$), and occupy the same region in the $(B-V)$ vs. V diagram as the LMC blue clusters (Fig. 12). The bluest objects are young nuclei of OB associations, which were included even though they differ from the stable open clusters. The color histogram shows a lack of red clusters relative to the LMC. This color distribution differs even more strongly from the colors of clusters in M33 (Christian and Schommer 1982, 1988) and, especially, in M31 (Hodge *et al.* 1987), where a larger fraction of clusters have $(B-V) > 0.5$.

In Fig. 13(a) the sequence of LMC clusters used for age calibration by Girardi *et al.* (1995) is indicated. Using their age calibration the clusters for which we could measure both $U-B$ and $B-V$ have ages between a few Myr and ∼500 Myr. No reddening correction has been applied, even though $E(B-V) \simeq 0.1$ could probably bring the data to a better fit to the LMC sequence. It seems appropriate to compare the M101 clusters with the cluster system of M33, also an Sc galaxy, studied in detail by Christian and Schommer (1988). Fig. 13(b) compares the $(B-V)$ vs. $(V-I)$ diagram for the two galaxies. The calibration line of Christian and Schommer (1988) is shown. The lack of M101 red clusters, having $(V-I) > 0.7$, is evident. It could be possible that this is an effect of the position in the galaxy where these clusters are found, *i.e.* close to the nucleus. In the M33 data, however, there is no indication that the red clusters preferentially lie away from the nucleus. The fractional area of M101 surveyed for clusters is too small to draw firm conclusions on the overall cluster population and on its differences relative to other galaxies. We however remind the reader that this area roughly equals the extent of the entire LMC. On the basis of our analysis we can only conclude that red clusters ("old globulars" candidates) are rare in the field studied. Many of the remaining clusters are very likely populous clusters of the same kind found in the LMC. The large ratio between the number of blue and red clusters is consistent with previous findings that populous clusters are preferentially found in late-type galaxies.

Two giant H II regions, numbers 972 and 1013 in the catalog of Hodge *et al.* (1990), fall in our HST field, corresponding to associations 57 and 72, respectively. Both have a high Hα luminosity, with a number of ionizing photons in excess of 10^{51} s^{-1} (Table 5). By comparison, 30 Dor in the LMC has an Hα luminosity corresponding to $\sim 10^{52}$ ionizing photons/s. The morphology of the

two regions differs somewhat. Region 72 resembles 30 Dor in having a bright, compact core cluster, which is probably responsible for most of the ionizing flux in the nebula. Several fainter clusters or single stars surround the central object. In region 57, on the contrary, we see a normal association of bright stars, similar in structure to the giant H II region NGC 604 in M33. To better quantify the properties of these embedded star clusters, and in order to compare them with similar objects in nearby galaxies, we measured fluxes in different apertures, centered on the brightest object in each of the two H II regions. In region 72, the radius of the core cluster is ∼22 pc, with a radius containing one-half the total light $R_{0.5} \simeq 7$ pc, and a total absolute magnitude $M_V = -12.3$. This object shows some finer structure, namely the presence of 2 distinct clusters, with a peak ratio of about 3:1. Each one has $R_{0.5} \simeq 3.6$ pc. The brightest component has a luminosity $M_V \simeq -12.0$, and a corresponding mean surface brightness $\Sigma_{0.5} = 6.9 \times 10^4\ L_{V,\odot}\ \mathrm{pc}^{-2}$ inside the radius $R_{0.5}$. This compares with $\Sigma_{0.5} = 1.3 \times 10^5\ L_{V,\odot}\ \mathrm{pc}^{-2}$, $R_{0.5} = 1.7$ pc and a total absolute magnitude $M_V = -11.1$ for R136 in 30 Dor (Hunter *et al.* 1995). Region 72 is therefore comparable to 30 Dor also quantitatively, even though it is somewhat less compact. We remind the reader that the "super star clusters" found in some galaxies (O'Connell *et al.* 1994) represent more extreme modes of star formation, 10–30 times more luminous than region 72, relative to the same age. In region 57 the main component is not as bright as in region 72, $M_V = -10.7$, while the nearby objects are typically 2 magnitudes fainter, and could be smaller clusters or very bright stars.

9. Conclusions

We have described an objective algorithm to identify 79 OB associations in an HST field of the galaxy M101. The following results were found:

1. The size distribution of the associations is comparable to that in the Magellanic Clouds, M33, NGC 6822 and M31, with a typical mean size of 90 pc;

2. The stellar luminosity function has a slope $d\log N/d\,V = 0.60 \pm 0.05$, both in the associations and in the general field;

3. H II regions tend to be slightly redder than the average OB association;

4. No indication that the upper mass limit of the IMF is lower than in low-metallicity environments is found;

5. Most of the star clusters identified in the field belong to the same class of populous clusters found in the LMC. Red clusters are rare.

We thank the HST Distance Scale Key Project team members, Abi Saha in particular, for their support in this work, Paul Hodge for his comments and Paul Scowen for providing us with unpublished material on H II regions. This work was supported by NASA through grant GO-2227-87A, and by the NSF through grants AST-9019150 and AST-9421145.

A. OB ASSOCIATIONS IN THE LMC

As a further application of the objective algorithm described in § 4, data on the LMC were analyzed. Stellar associations in the LMC were catalogued from wide-field photographic plates by Lucke and Hodge (1970) and the characteristics of the 122 associations in the catalog were studied by Hodge and Lucke (1970). We applied the clustering algorithm to the catalog of bright stars of Rousseau *et al.* (1978) (in the updated machine-readable form available through the NASA Astronomical Data Center). It is interesting to compare our numerical association-finding technique with subjective human intelligence when applied to the nearest galaxy, where a resolution of less than a pc ($1''= 0.24$ pc) is attainable.

Stars were selected with two different criteria, based on spectral type (all catalogued stars with type earlier than B2.5) and on photometric parameters ($V< 13.7$, $B-V< 0.15$, to match the criteria adopted for M101 and M33). The two sets of stars gave approximately the same results, so the following discussion concentrates on the photometrically selected one. The search radius determined by the algorithm is 60 pc (the same used by Battinelli (1991) in the SMC). Out of the 1354 "blue" stars, 725 are distributed in 121 associations. The resulting average size is 78 pc, the same value found by Hodge and Lucke (1970). This includes all agglomerations of stars with at least 3 stars. A correction, based on the expected contamination by statistical fluctuations, gives 94 pc instead. The distribution of association sizes is shown in Fig. 14 for both Hodge and Lucke's data and this work. They appear remarkably similar, except for a larger number of small associations in Hodge and Lucke. Regarding the case-by-case comparison (Fig. 15), the agreement is far from good. It has been noted (Caplan and Deharveng 1986) that the stars in the Rousseau *et al.* catalog, which is based on an objective prism spectral survey, show no concentration towards H II regions, and we infer that the catalog is under-representing the regions richest in OB stars, which may be the explanation for the poor agreement. For the purpose of making an objective catalog of associations in the LMC a better catalog of the brightest blue stars is needed.

Table 1. Median photometric errors.

V	σ_V	σ_I	σ_B	σ_U
20–21	0.031	0.044	0.094	0.115
21–22	0.034	0.048	0.117	0.149
22–23	0.038	0.062	0.125	0.157
23–24	0.048	0.085	0.165	0.202
24–25	0.061	0.122	0.235	0.285
25–26	0.080	0.181	0.361	0.432
26–27	0.107	0.242	0.529	0.618

Table 2. Slope of the luminosity function.

Color criterion	field + association s	field	associations
$U-V < -0.5$	0.58 ± 0.04	0.58 ± 0.05	0.58 ± 0.06
$U-B < -0.7$	0.62 ± 0.04	0.62 ± 0.05	0.62 ± 0.07
$B-V < +0.4$	0.55 ± 0.04	0.57 ± 0.04	0.53 ± 0.05

Table 3. Properties of OB associations.

ID	RA (14^h)	DEC ($+54°$)	Diameter (pc)	N_{blue}	N_{tot}	E(B−V)	age (Myr)
1	$3^m\ 25^s.1$	$21'\ 10''$	21	11	15	0	14
2	$3^m\ 23^s.2$	$21'\ 25''$	103	12	35	0.3	5
3	$3^m\ 24^s.4$	$21'\ 05''$	29	6	12	0.3	5
4	$3^m\ 24^s.1$	$21'\ 02''$	61	16	45	0.4	4
5	$3^m\ 24^s.2$	$20'\ 55''$	72	14	26	0.4	6
6	$3^m\ 23^s.9$	$21'\ 00''$	118	11	29	0.3	3
7	$3^m\ 22^s.4$	$21'\ 11''$	62	6	8	0.2	6
8	$3^m\ 17^s.6$	$21'\ 00''$	119	10	25	0.2	8
9	$3^m\ 17^s.9$	$21'\ 06''$	306	49	125	0.2	5
10	$3^m\ 18^s.8$	$21'\ 23''$	126	12	24	0.3	5
11	$3^m\ 21^s.6$	$21'\ 45''$	96	10	18	0.2	4
12	$3^m\ 16^s.6$	$21'\ 13''$	80	10	16	0.2	5
13	$3^m\ 19^s.7$	$21'\ 44''$	89	11	20	0.2	4
14	$3^m\ 15^s.8$	$21'\ 24''$	108	8	15	0.2	4
15	$3^m\ 17^s.8$	$21'\ 42''$	113	14	26	0.2	6
16	$3^m\ 17^s.0$	$21'\ 41''$	127	12	28	0.3	4
17	$3^m\ 16^s.0$	$21'\ 45''$	129	24	39	0.1	4
18	$3^m\ 15^s.7$	$21'\ 46''$	154	9	15	0.1	6
19	$3^m\ 18^s.1$	$22'\ 04''$	111	10	19	0.2	4
20	$3^m\ 15^s.6$	$21'\ 52''$	226	21	63	0.2	6
21	$3^m\ 15^s.0$	$21'\ 51''$	43	11	12	0.1	4
22	$3^m\ 13^s.1$	$21'\ 50''$	173	15	30	0.2	6
23	$3^m\ 18^s.1$	$22'\ 20''$	128	8	12	0.1	7
24	$3^m\ 12^s.6$	$21'\ 46''$	121	15	30	0.2	7
25	$3^m\ 13^s.1$	$21'\ 53''$	59	7	8	0.3	4
26	$3^m\ 12^s.6$	$21'\ 55''$	77	7	10	0.1	6
27	$3^m\ 18^s.4$	$22'\ 33''$	143	16	21	0.2	7
28	$3^m\ 21^s.4$	$22'\ 42''$	125	10	23	0.1	6
29	$3^m\ 24^s.3$	$22'\ 12''$	78	9	15	0.2	3
30	$3^m\ 26^s.3$	$22'\ 00''$	105	8	21	0.3	6
31	$3^m\ 25^s.7$	$22'\ 14''$	231	30	65	0.3	4
32	$3^m\ 26^s.1$	$22'\ 11''$	181	22	40	0.2	4
33	$3^m\ 26^s.8$	$22'\ 04''$	102	10	19	0.2	7
34	$3^m\ 25^s.9$	$22'\ 26''$	117	10	18	0.2	6
35	$3^m\ 23^s.6$	$22'\ 55''$	74	9	11	0.2	10
36	$3^m\ 25^s.4$	$22'\ 43''$	162	17	34	0.2	6

Table 3—Continued

ID	RA (14^h)	DEC (+54°)	Diameter (pc)	N_{blue}	N_{tot}	E(B−V)	age (Myr)
37	3^m $24^s.6$	22′ 55″	232	27	101	0.3	4
38	3^m $28^s.3$	22′ 08″	141	9	20	0.4	4
39	3^m $25^s.5$	22′ 55″	83	7	11	0.2	4
40	3^m $25^s.3$	21′ 16″	68	10	17	0.3	4
41	3^m $24^s.6$	21′ 24″	83	10	15	0.1	7
42	3^m $25^s.2$	21′ 15″	59	8	13	0	14
43	3^m $25^s.6$	21′ 10″	80	9	15	0.2	6
44	3^m $25^s.3$	21′ 12″	93	10	17	0.2	6
45	3^m $25^s.5$	21′ 08″	94	8	16	0.2	7
46	3^m $24^s.4$	21′ 22″	66	11	16	0	11
47	3^m $25^s.7$	21′ 05″	51	9	9	0.2	4
48	3^m $25^s.1$	21′ 13″	59	10	13	0.3	8
49	3^m $25^s.8$	21′ 04″	38	8	9	0.1	6
50	3^m $25^s.6$	21′ 06″	80	7	15	0.3	7
51	3^m $23^s.7$	21′ 22″	126	23	41	0.3	3
52	3^m $23^s.4$	21′ 26″	46	8	11	0.3	8
53	3^m $23^s.5$	21′ 25″	49	8	10	0.2	4
54	3^m $23^s.9$	21′ 19″	140	19	37	0.3	5
55	3^m $23^s.8$	21′ 18″	91	10	15	0.2	9
56	3^m $23^s.7$	21′ 20″	59	7	10	0.2	5
57	3^m $23^s.7$	21′ 16″	203	105	175	0.2	3
58	3^m $24^s.0$	21′ 14″	89	12	21	0.2	7
59	3^m $24^s.1$	21′ 13″	53	8	10	0	9
60	3^m $24^s.2$	21′ 11″	53	11	12	0.4	4
61	3^m $23^s.1$	21′ 21″	99	23	36	0.2	4
62	3^m $23^s.2$	21′ 16″	76	13	31	0.3	7
63	3^m $23^s.3$	21′ 15″	133	22	50	0.2	6
64	3^m $23^s.0$	21′ 18″	122	22	41	0.3	4
65	3^m $23^s.1$	21′ 17″	77	13	14	0.2	5
66	3^m $23^s.2$	21′ 14″	79	9	12	0.3	7
67	3^m $24^s.0$	21′ 05″	71	12	19	0.3	6
68	3^m $22^s.7$	21′ 16″	230	47	116	0.3	4
69	3^m $22^s.6$	21′ 17″	74	9	11	0.1	7
70	3^m $22^s.7$	21′ 08″	98	11	24	0.2	5
71	3^m $22^s.8$	21′ 09″	88	14	23	0.1	6
72	3^m $22^s.8$	21′ 04″	241	88	221	0.2	3

Table 3—Continued

ID	RA (14^h)	DEC ($+54°$)	Diameter (pc)	N_{blue}	N_{tot}	E(B−V)	age (Myr)
73	$3^m\ 22\overset{s}{.}0$	$21'\ 09''$	82	10	19	0.3	7
74	$3^m\ 21\overset{s}{.}5$	$21'\ 13''$	61	7	9	0.2	7
75	$3^m\ 21\overset{s}{.}6$	$21'\ 11''$	65	8	12	0	12
76	$3^m\ 21\overset{s}{.}4$	$21'\ 13''$	59	8	10	0.2	7
77	$3^m\ 21\overset{s}{.}2$	$21'\ 15''$	71	15	22	0.3	5
78	$3^m\ 21\overset{s}{.}5$	$21'\ 12''$	67	7	12	0.2	10
79	$3^m\ 21\overset{s}{.}1$	$21'\ 13''$	68	7	8	0.2	9

[a]Diameters are for a distance of 7.4 Mpc

Table 4. Comparison of OB associations properties.

Galaxy	average diameter (pc)	median diameter (pc)	minimum no. of stars
M 101	100	90	7
LMC	80	60	3
SMC	90	70	3
M 33	80	60	10
M 31	120	100	5
NGC 6822	90	90	10

Table 5. Balmer decrement reddening and number of ionizing photons.

Association no.	E$(B-V)$	log Q_0
4	0.82	50.91
11	0.19	49.91
13	0.29	50.33
31	0.29	50.22
36	0.36	49.88
41	0.14	49.25
51	0.19	49.91
52	0.41	49.71
57	0.24	51.17
61	0.47	50.27
67	0.25	50.12
68	0.39	50.94
72	0.29	51.92

Table 6. Cluster photometry.

ID	RA (14^h)	DEC ($+54°$)	V	U-B	B-V	V-I
1	$3^m\ 25\overset{s}{.}3$	$21'\ 11''$	20.51	-0.50	0.21	0.55
2	$3^m\ 25\overset{s}{.}5$	$21'\ 06''$	20.93	-0.80	0.26	0.51
3	$3^m\ 23\overset{s}{.}7$	$21'\ 14''$	23.26	···	0.58	0.67
4	$3^m\ 22\overset{s}{.}4$	$21'\ 05''$	23.71	···	0.24	0.45
5	$3^m\ 23\overset{s}{.}4$	$21'\ 28''$	21.59	···	0.38	0.60
6	$3^m\ 22\overset{s}{.}7$	$20'\ 58''$	22.48	···	0.30	0.49
7	$3^m\ 25\overset{s}{.}0$	$21'\ 12''$	22.29	···	0.31	0.53
8	$3^m\ 25\overset{s}{.}3$	$21'\ 08''$	22.51	···	0.06	0.39
9	$3^m\ 24\overset{s}{.}6$	$21'\ 04''$	22.07	-0.67	0.29	0.55
10	$3^m\ 19\overset{s}{.}9$	$21'\ 13''$	22.31	-0.23	0.10	0.36
11	$3^m\ 16\overset{s}{.}9$	$21'\ 19''$	21.88	-0.07	0.33	0.62
12	$3^m\ 18\overset{s}{.}7$	$22'\ 33''$	20.86	-0.79	-0.18	0.09
13	$3^m\ 21\overset{s}{.}9$	$21'\ 45''$	20.45	-0.89	-0.02	0.34
14	$3^m\ 15\overset{s}{.}6$	$22'\ 13''$	21.00	0.34	0.27	0.58
15	$3^m\ 14\overset{s}{.}1$	$22'\ 05''$	20.95	-0.27	0.12	0.52
16	$3^m\ 17\overset{s}{.}7$	$22'\ 09''$	21.27	0.11	0.25	0.71
17	$3^m\ 19\overset{s}{.}7$	$21'\ 40''$	20.04	···	1.01	1.08
18	$3^m\ 18\overset{s}{.}5$	$22'\ 33''$	21.65	0.04	0.43	0.59
19	$3^m\ 22\overset{s}{.}2$	$22'\ 49''$	21.52	-0.41	0.16	0.60
20	$3^m\ 25\overset{s}{.}6$	$22'\ 41''$	21.00	-0.06	0.20	0.37
21	$3^m\ 27\overset{s}{.}4$	$22'\ 15''$	21.76	-0.50	0.13	0.68
22	$3^m\ 26\overset{s}{.}4$	$21'\ 58''$	21.71	-0.66	0.30	0.99
23	$3^m\ 29\overset{s}{.}7$	$22'\ 24''$	20.84	0.09	0.35	0.65
24	$3^m\ 29\overset{s}{.}3$	$22'\ 19''$	21.35	···	0.46	0.72
25	$3^m\ 28\overset{s}{.}4$	$22'\ 19''$	22.26	···	0.39	0.66
26	$3^m\ 22\overset{s}{.}2$	$22'\ 37''$	21.74	···	0.46	0.97
27	$3^m\ 24\overset{s}{.}1$	$21'\ 43''$	21.85	-0.93	-0.07	0.48
28	$3^m\ 24\overset{s}{.}1$	$21'\ 57''$	22.10	-1.00	0.05	0.29
29	$3^m\ 25\overset{s}{.}7$	$22'\ 09''$	21.53	-0.97	-0.02	0.31
30	$3^m\ 24\overset{s}{.}2$	$20'\ 56''$	20.50	-0.06	0.22	0.55
31	$3^m\ 24\overset{s}{.}2$	$21'\ 10''$	20.46	-0.61	0.29	0.69
32	$3^m\ 24\overset{s}{.}0$	$21'\ 12''$	20.56	-0.51	0.38	0.59
33	$3^m\ 22\overset{s}{.}3$	$21'\ 12''$	22.34	···	0.99	1.01
34	$3^m\ 24\overset{s}{.}0$	$21'\ 23''$	19.58	···	1.14	1.47
35	$3^m\ 21\overset{s}{.}8$	$21'\ 05''$	20.76	0.33	0.44	0.70
36	$3^m\ 24\overset{s}{.}8$	$21'\ 11''$	21.49	0.17	0.78	1.19

Table 6—Continued

ID	RA (14^h)	DEC ($+54°$)	V	U-B	B-V	V-I
37	$3^m\ 24\overset{s}{.}6$	$21'\ 11''$	21.59	0.01	0.27	0.54
38	$3^m\ 24\overset{s}{.}5$	$21'\ 02''$	21.48	-0.35	0.38	0.60
39	$3^m\ 24\overset{s}{.}9$	$21'\ 11''$	21.91	-0.47	0.42	0.69
40	$3^m\ 23\overset{s}{.}3$	$20'\ 53''$	21.46	-0.42	0.29	0.55
41	$3^m\ 23\overset{s}{.}2$	$21'\ 01''$	22.03	···	0.51	0.82
42[1]	$3^m\ 22\overset{s}{.}8$	$21'\ 04''$	17.71	-1.10	0.08	0.05
43[2]	$3^m\ 23\overset{s}{.}7$	$21'\ 16''$	19.38	-1.05	0.25	-0.09

[1]H II region core cluster, in association 72

[2]H II region core cluster, in association 57

REFERENCES

Battinelli, P. 1991, A&A, 244, 69

Berkhuijsen, E. M. and Humphreys, R. M. 1989, A&A, 214, 68

Blaauw, A. 1991, The Physics of Star Formation and Early Stellar Evolution, p. 125, eds. C. J. Lada and N. D. Kylafis

Blaha, C. and Humphreys, R. M. 1989, AJ, 98, 1598

Caplan, J. and Deharveng, L. 1986, A&A, 155, 297

Christian, C. A., and Schommer, R. A. 1988, AJ, 95, 704

Christian, C. A., and Schommer, R. A. 1982, ApJS, 49, 405

de Vaucouleurs, G., de Vaucouleurs, A., Corwin, H. G., Buta, R. J., Paturel, G., and Fouque, P. 1991, Third Reference Catalogue of Bright Galaxies (New York: Springer-Verlag)

Doom, C., De Greeve, J. P. and de Loore, C. 1985, ApJ, 290, 185

Efremov, Y. N., and Chernin, A. D. 1994, Vistas in Astronomy, 38, 165

Efremov, Y. N., Ivanov, G. R., and Nokolov, N. S. 1987, Ap&SS, 135, 119

FitzGerald, M. P. 1970, A&A, 4, 234

Fitzpatrick, E. L. and Garmany, C. D. 1990, ApJ, 363, 119

Freedman, W. 1985, ApJ, 299, 74

Garmany, C. D. 1994, PASP, 106, 25

Garmany, C. D., and Stencel, R. E. 1992, A&ASS, 94, 211

Girardi, L., Chiosi, C., Bertelli, G., and Bressan, A. 1995, A&A, 298, 87

Haiman, Z., Magnier, E. A., Battinelli, P., Lewin, W. H. G., van Paradijs, J., Hasinger, G., Pietsch, W., Supper, R. and Trümper, J. 1994, A&A, 290, 371

Hodge, P. W., Gurwell, M., Goldader, J. D., and Kennicutt, R. C. 1990, ApJS, 73, 661

Hodge, P. W., Mateo, M., Lee, M. G., and Geisler, D. 1987, PASP, 98, 173

Hodge, P. 1986, Luminous Stars and Associations in Galaxies, (IAU Symposium No. 116), eds. C. W. H. de Loore, A. J. Willis, and P. Laskarides (Reidel, Boston), p. 369

Hodge, P. W. 1985, PASP, 97, 530

Hodge, P. W. and Lucke, P. B. 1970, AJ, 75, 933

Holtzman, J. A., Burrows, C. J., Casertano, S., Hester, J. J., Trauger, J. T., Watson, A. M. and Worthey, G. 1995, PASP, 107, 1065

Hughes, S. M. G., *et al.* 1994, ApJ, 428, 143

Humphreys, R. M. 1978, ApJS, 38, 309

Hunter, D. A., and Thronson, H. A. 1995, ApJ, 452, 238

Hunter, D. A., Shaya, E. J., Holtzman, J. A., Light, R. M., O'Neil, E. J., and Lynds, R. 1995, ApJ, 448, 179

Janes, K. A., Tilley, C., and Lynga, G. 1988, AJ, 95, 771

Kelson, D. *et al.* 1996, ApJ, in press

Kennicutt, R. C. and Garnett, D. R. 1996, ApJ, 456, 504

Kennicutt, R. C., Freedman, W. L., and Mould, J. R. 1995, AJ, 110, 1476

Kennicutt, R. C. and Chu, Y.-H. 1988, AJ, 95, 720

Kennicutt, R. C. 1984, ApJ, 287, 116

Leitherer, C. and Heckman, T. 1995, ApJS, 96, 9L

Lucke, P. B. and Hodge, P. W. 1970, AJ, 75, 171

Magnier, E. A., Battinelli, P., Lewin, W. H. G., Haiman, Z., van Paradijs, J., Hasinger, G., Pietsch, W., Supper, R., and Trümper, J. 1993, A&A, 278, 36

Massey, P., Johnson, K. E., and DeGioia-Eastwood, K. 1995b, ApJ, 454, 151

Massey, P., Lang, C. C., DeGioia-Eastwood, K. and Garmany, C. D. 1995a, ApJ, 438, 188

Massey, P., Garmany, C. D., Silkey, M., and DeGioia-Eastwood, K. 1989, AJ, 97, 107

Massey, P. 1985, PASP, 97, 5

Meynet, G., Mermillod, J.-C., and Maeder, A. 1993, A&A, 98, 477

O'Connell, R. W., Gallagher, J. S., and Hunter, D. A. 1994, ApJ, 433, 65

Osterbrock, D. E. 1989, Astrophysics of Gaseous Nebulae and Active Galactic Nuclei (University Science Books, Mill Valley)

Regan, M. W. and Wilson, C. D. 1993, AJ, 105, 499

Rosa, M. R. and Benvenuti, P. 1994, A&A, 291, 1

Rousseau, J., Martin, N., Prévot, L., Rebeirot, E., Robin, A., and Brunet, J. P. 1978, A&AS, 31, 243

Schaller, G., Schaerer, D., Meynet, G. and Maeder, A. 1992, A&ASS, 96, 269

Seaton, M. J. 1979, MNRAS, 187, 73

Shields, G. A. and Tinsley, B. M. 1976, ApJ, 203, 66

Stetson *et al.* 1996, in preparation

Stetson, P. 1994, PASP, 106, 250

van den Bergh, S. 1991, ApJ, 369, 1

ven den Bergh, S. 1981, A&A, 46, 79

Wilson, C. D. 1992, AJ, 104, 1374

Wilson, C. D. 1991, AJ, 101, 1663

This preprint was prepared with the AAS LaTeX macros v4.0.

Fig. 1.— Mosaic of the four WFPC2 chips. H II regions 1013 and 972 from the catalog of Hodge *et al.* (1990) are the brightest objects in chip 4 (upper right)(courtesy A. Turner).

Fig. 2.— Hα (line + continuum) image of M101 showing the HST field studied in this work. North is at the top.

Fig. 3.— Color-magnitude diagram of the M101 field with evolutionary tracks from Schaller *et al.* (1992), reddened by 0.21 mag in $(B-V)$. *(Inset)* The stars brighter than $V=22$ that appear in relatively uncrowded regions are shown with their individual photometric errors.

Fig. 4.— Outlines of the 79 OB associations which were found by applying the objective clustering algorithm. Stars having $(B-V)<0.4$ and $V<25.5$ are plotted.

Fig. 5.— Comparison of associations size distribution for M101, LMC, SMC, M31, NGC 6822 and M33.

Fig. 6.— The differential V luminosity function for the brightest stars in the associations. Only stars having $(U-V)<-0.5$ are included.

Fig. 7.— (a) E$(B-V)$ for all OB associations (measured by the reddening-free parameter Q=$(U-B)-0.72\,(B-V)$) and for all the bright H II regions found in the M101 field (measured by the Balmer decrement). (b) E$(B-V)$ for those associations for which both Q and the Balmer decrement were measured.

Fig. 8.— Color-magnitude diagram for the stars within the OB associations boundaries. For each association the stars have been dereddened according to the average E$(B-V)$ value measured from the Q parameter.

Fig. 9.— $(U-B)$ *vs* $(B-V)$ diagram for those stars in associations having internal photometric errors smaller than 0.15 mag in each band. The reddening correction has been applied as in Fig. 8. The main sequence and supergiants sequence are plotted, together with two lines of constant $U-V$ color (-0.9, supergiants of spectral type B5, and -0.4, at the transition between late B and early A supergiants). The arrow represents the reddening vector for a B0 supergiant.

Fig. 10.— (a) Example of age determination: theoretical isochrones from the Schaller *et al.* (1992) models from 2.5 to 9.5 Myr in steps of 1 Myr are superposed on the dereddened CMD of association 37. In this case an age of 4 Myr ($\pm$2 Myr) was estimated. (b) Number of blue stars in the associations vs. age. (c) Diameter of the associations vs. age. (d) Number of ionizing photons (measured from the Hα flux) vs. age. In these plots the estimated uncertainty of $\pm$2 Myr is represented by elongated bars.

Fig. 11.— The integrated and dereddened colors of the richest associations ($N_{\rm blue}>15$) compared to Leitherer and Heckman's (1995) population models for an instantaneous burst at solar metallicity. The dots represent the observed colors and the assigned ages. The two lines are for a Salpeter IMF

with high-mass limits of 100 and 30 $M_{\odot}$.

Fig. 12.— (a) $(B-V)$ vs. V integrated color-magnitude diagram for star clusters in M101 (open circles) and in the LMC (dots, from van den Bergh 1981); (b) color distribution for M101 (hatched) and LMC clusters.

Fig. 13.— (a) $(B-V)$ vs. $(U-B)$ integrated color-color diagram for the M101 clusters. The sequence of LMC clusters from Girardi *et al.* (1995) is indicated; (b) $(V-I)$ vs. $(B-V)$ diagram for clusters in M101 (open circles) and M33 (dots). The theoretical sequence shown is taken from Christian and Schommer (1988).

Fig. 14.— Histogram of the sizes of the associations in the LMC as determined by the objective algorithm (continuous line) and those found by Lucke and Hodge (dashed line). In the latter case more small agglomerations were found, and less for sizes of 80-100 pc. In general, though, the two distributions are very similar.

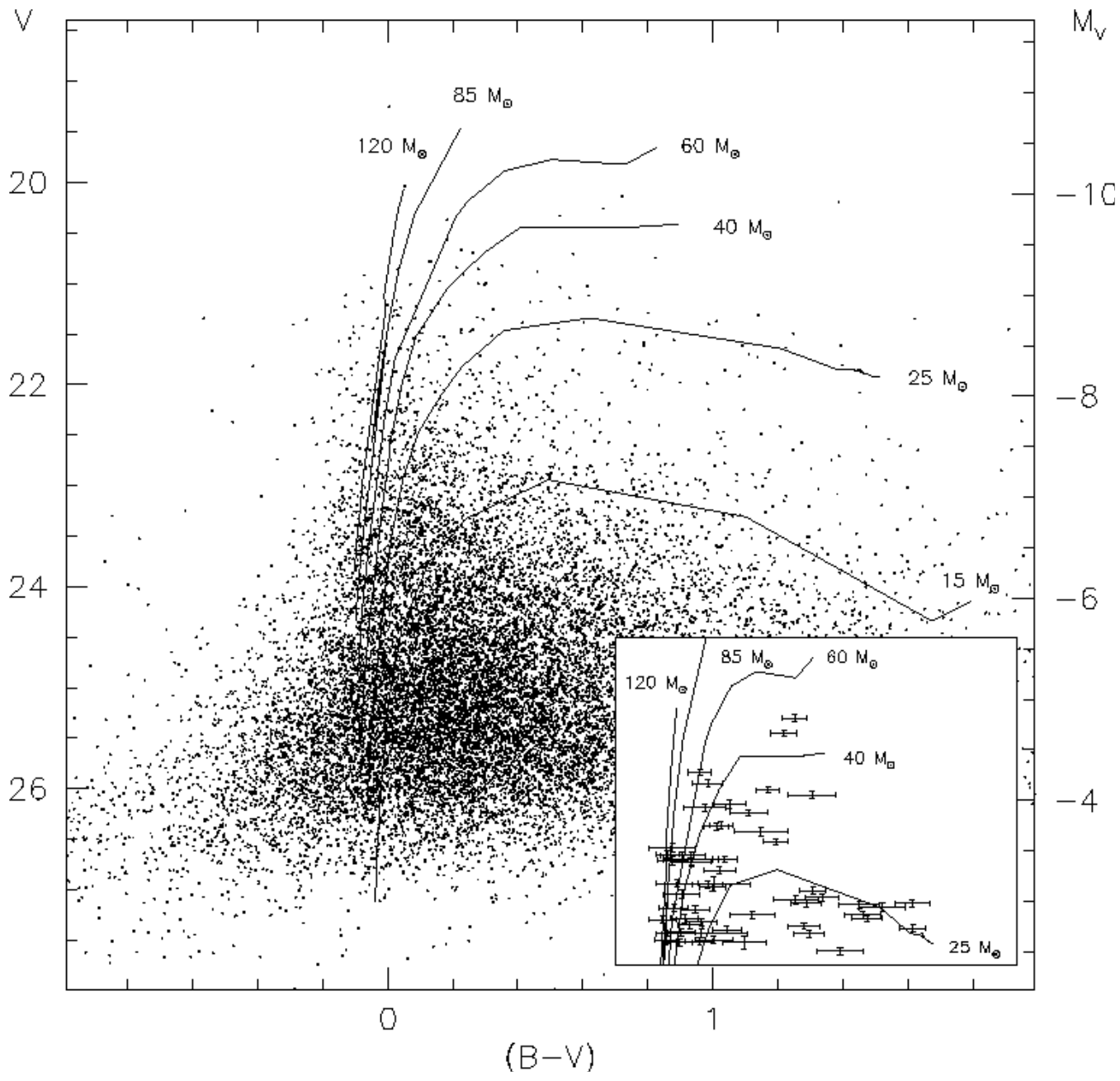
Fig. 15.— This map shows the LMC association boundaries determined by the objective algorithm (irregular polygons) together with the associations in the Lucke and Hodge (1970) catalog (circles). Although there are several matching cases, many discrepancies are present. This is likely to be due to the incompleteness of the bright LMC stars catalog in the densest regions and in correspondence of H II regions.

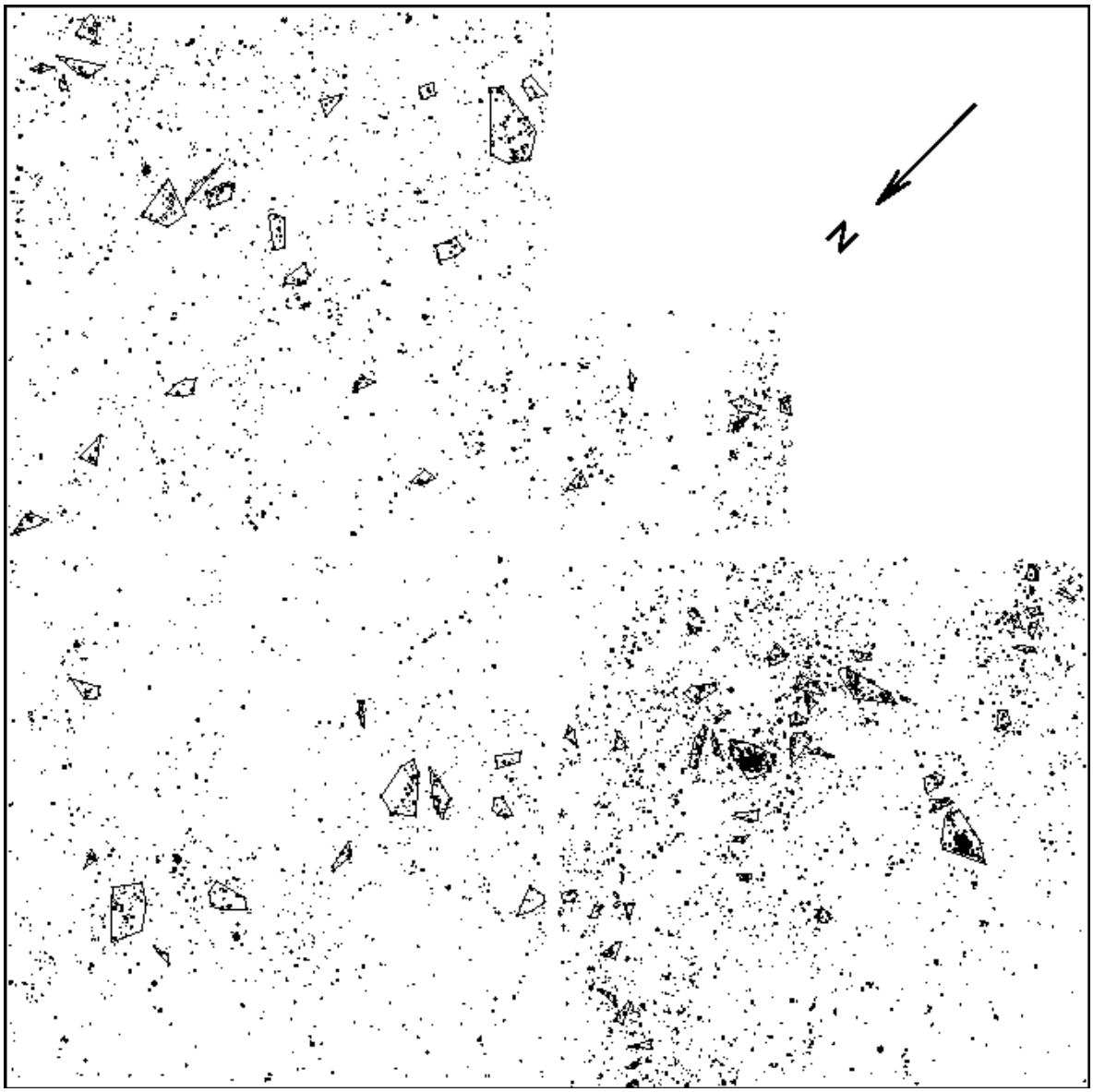
This figure "FIG1.jpg" is available in "jpg" format from:

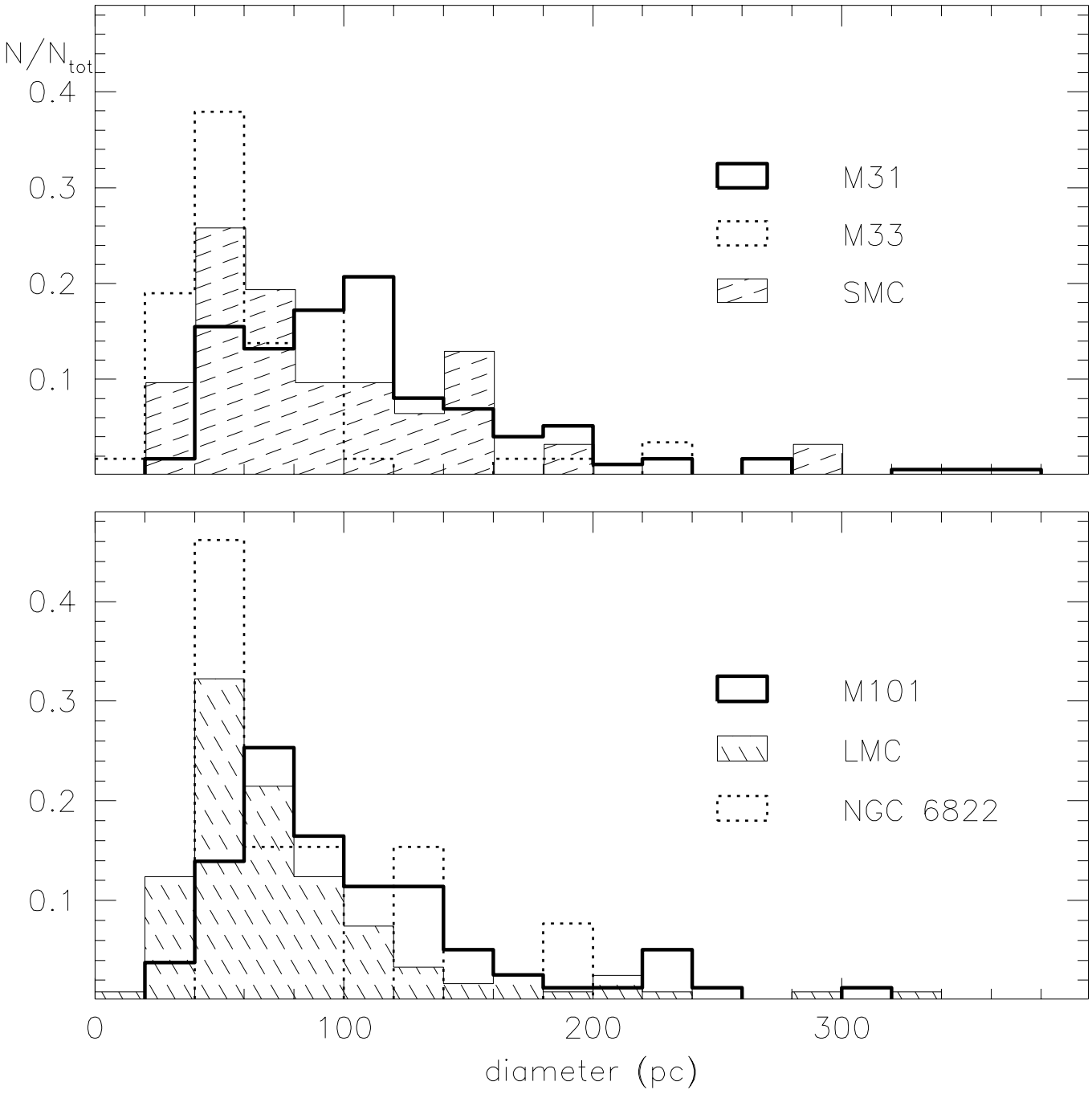
http://arxiv.org/ps/astro-ph/9606050v1

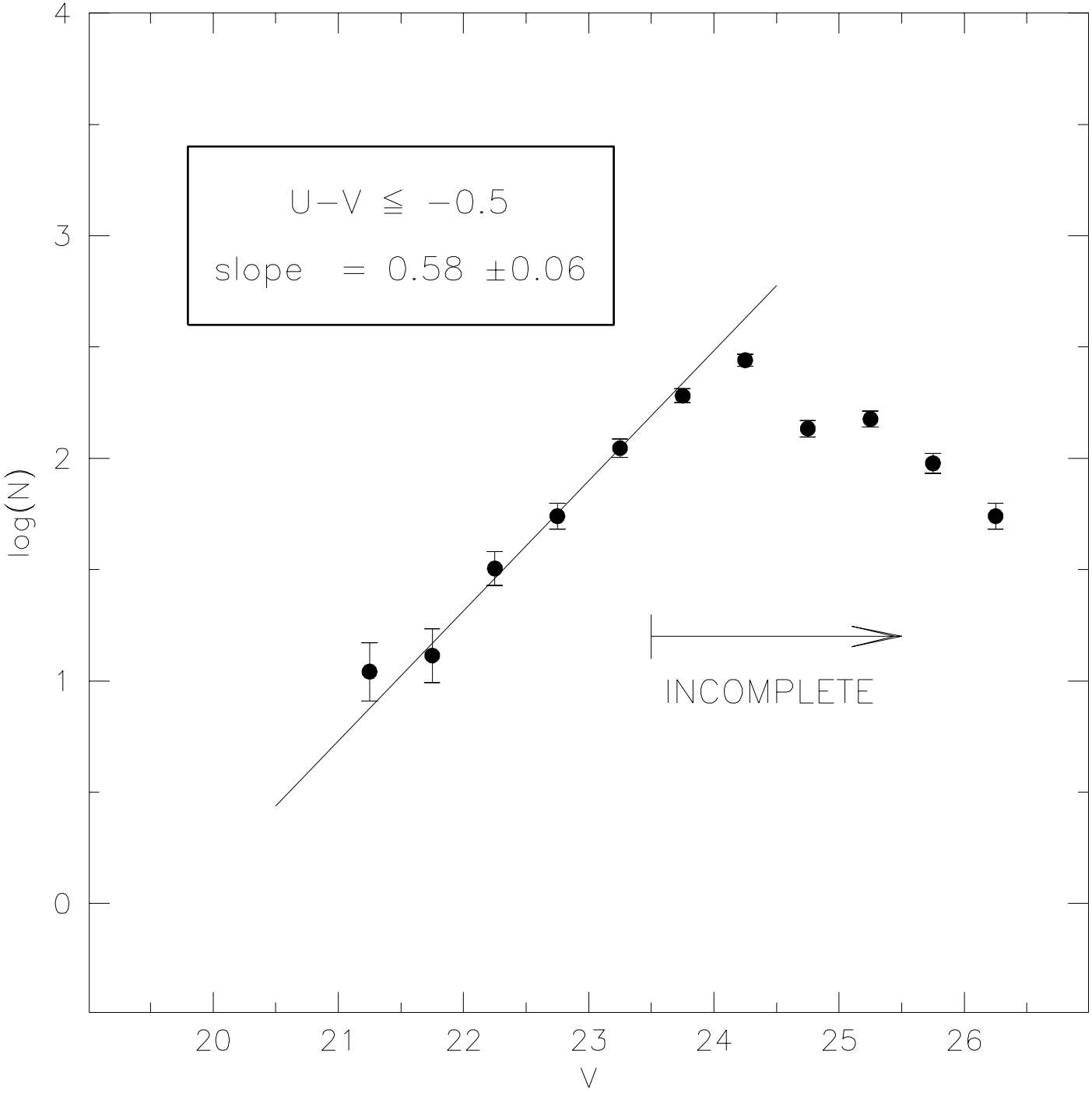
This figure "FIG2.jpg" is available in "jpg" format from:

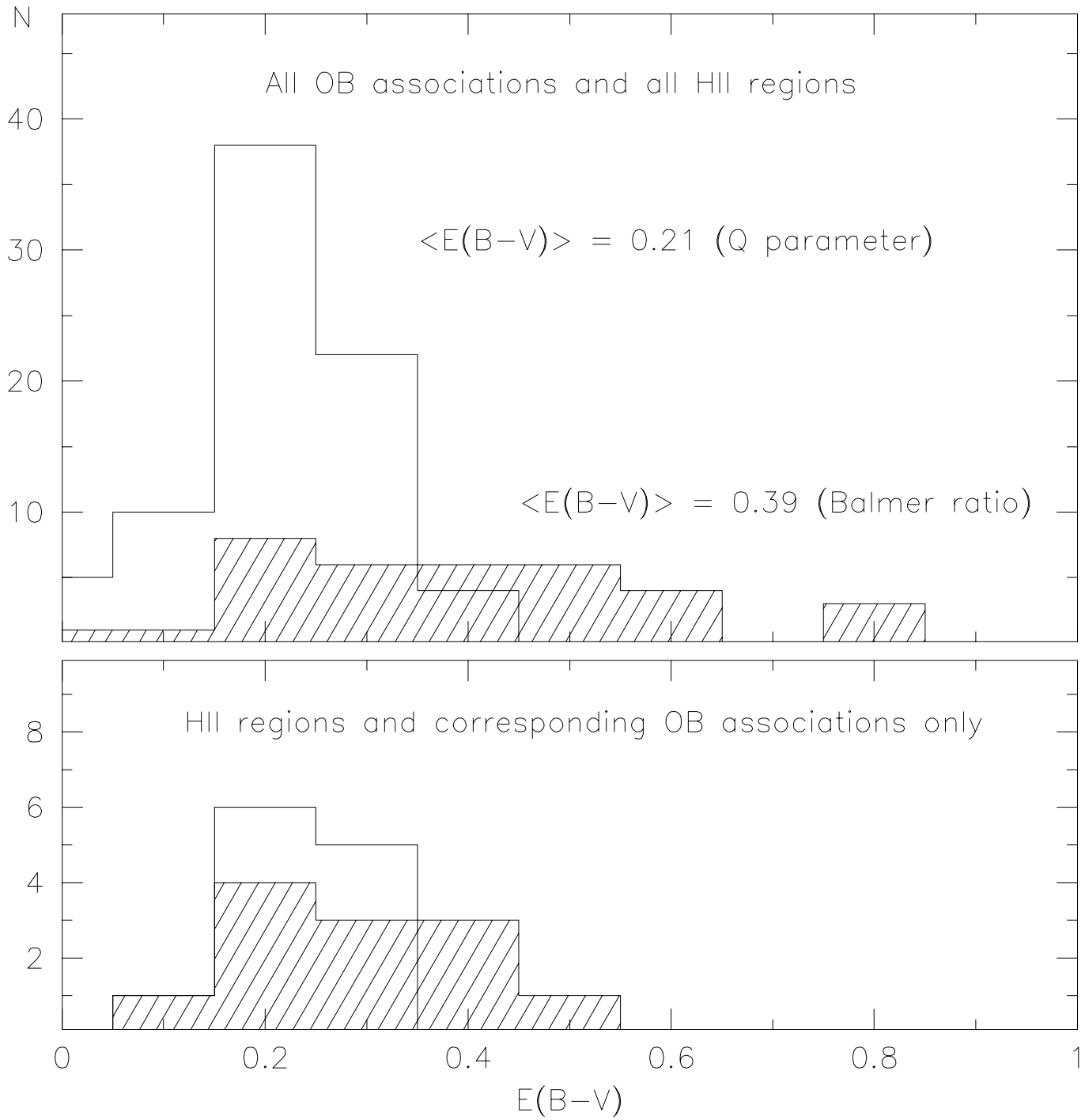
http://arxiv.org/ps/astro-ph/9606050v1

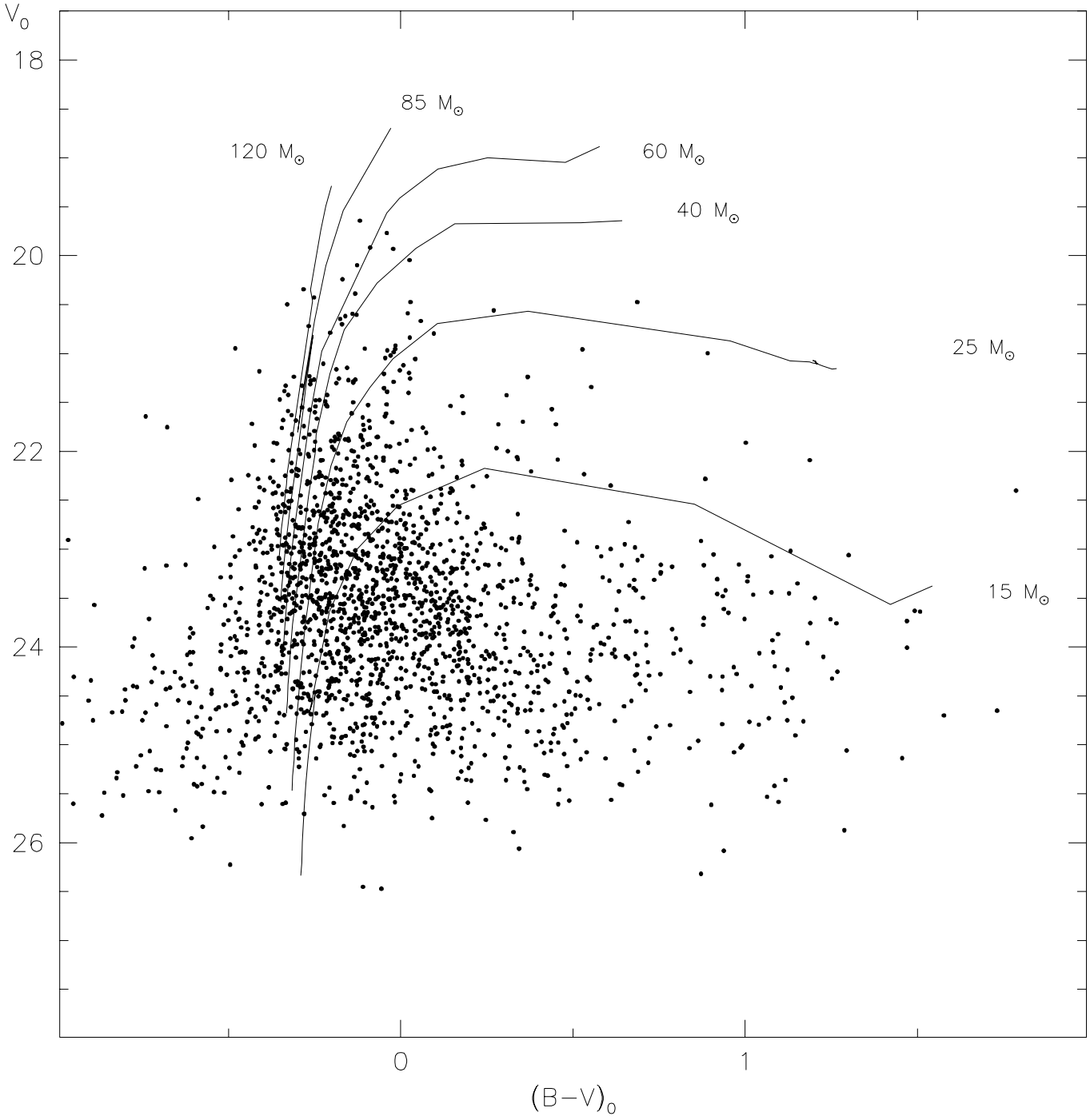

V
M_V
85 M⊙
120 M⊙
60 M⊙
40 M⊙
25 M⊙
15 M⊙
20
22
24
26
−10
−8
−6
−4
0
1
(B−V)

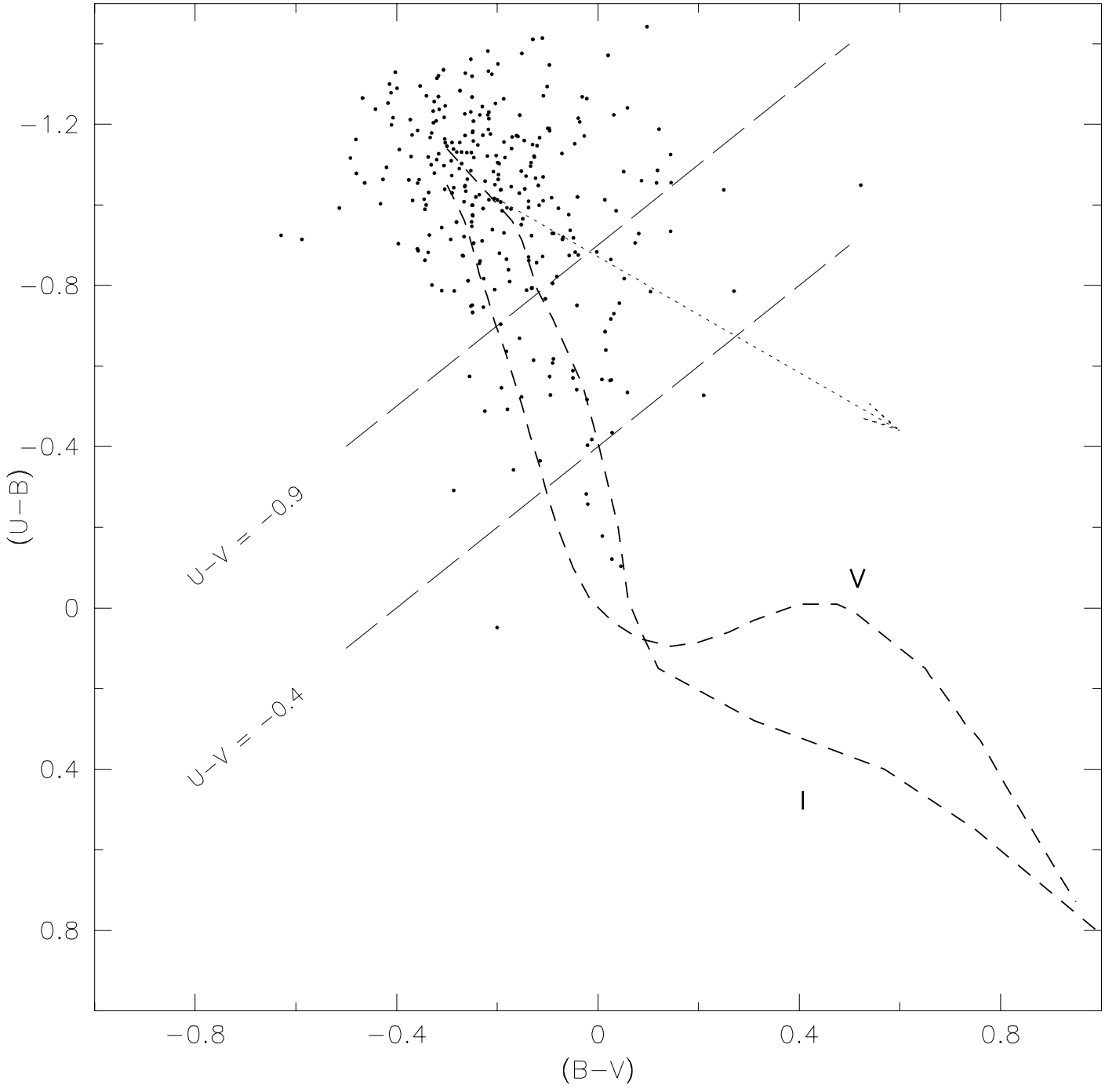

N

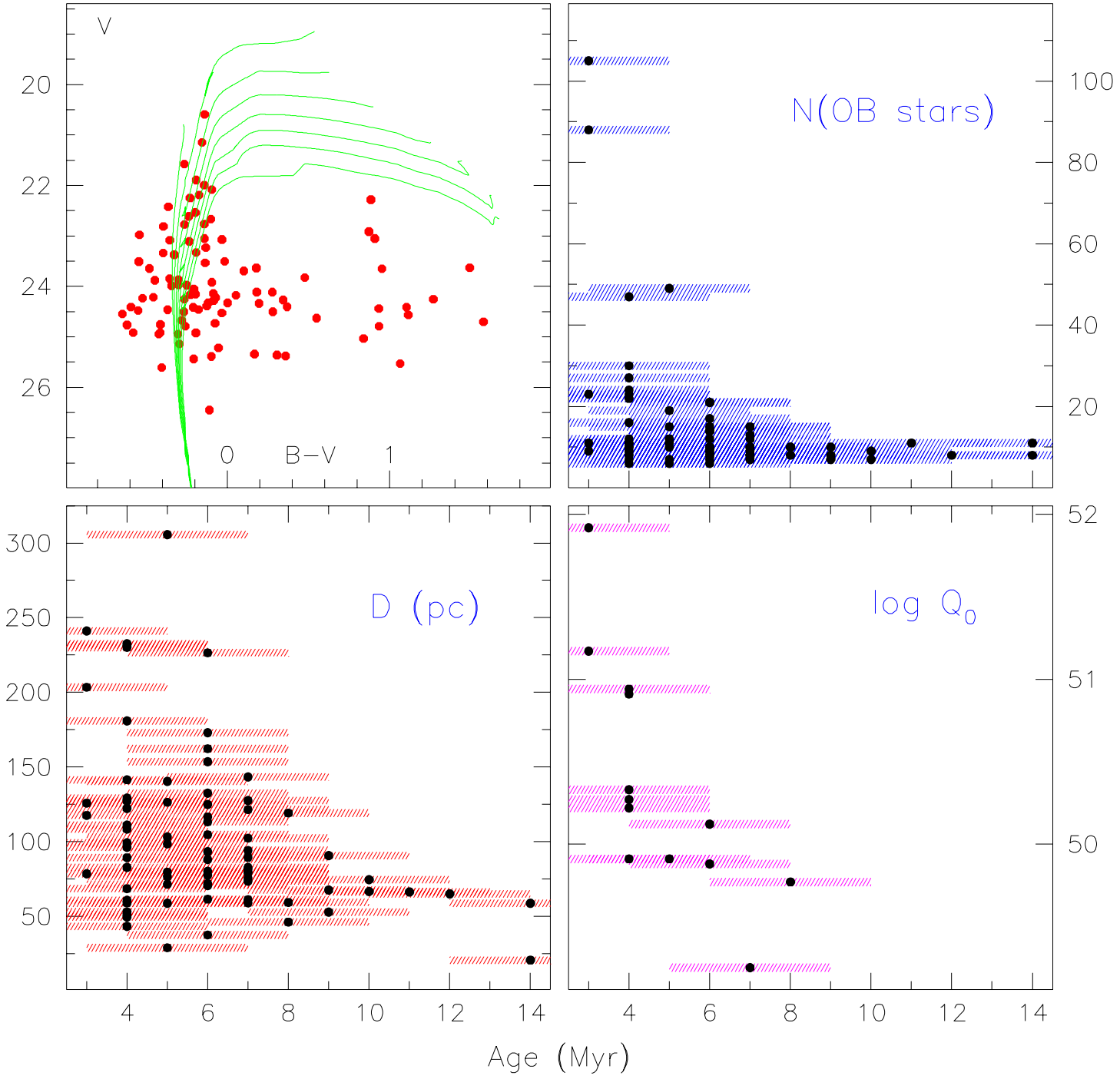

N/N_tot
0.4
0.3
0.2
0.1
M31
M33
SMC
0.4
0.3
0.2
0.1
M101
LMC
NGC 6822
0
100
200
300
diameter (pc)

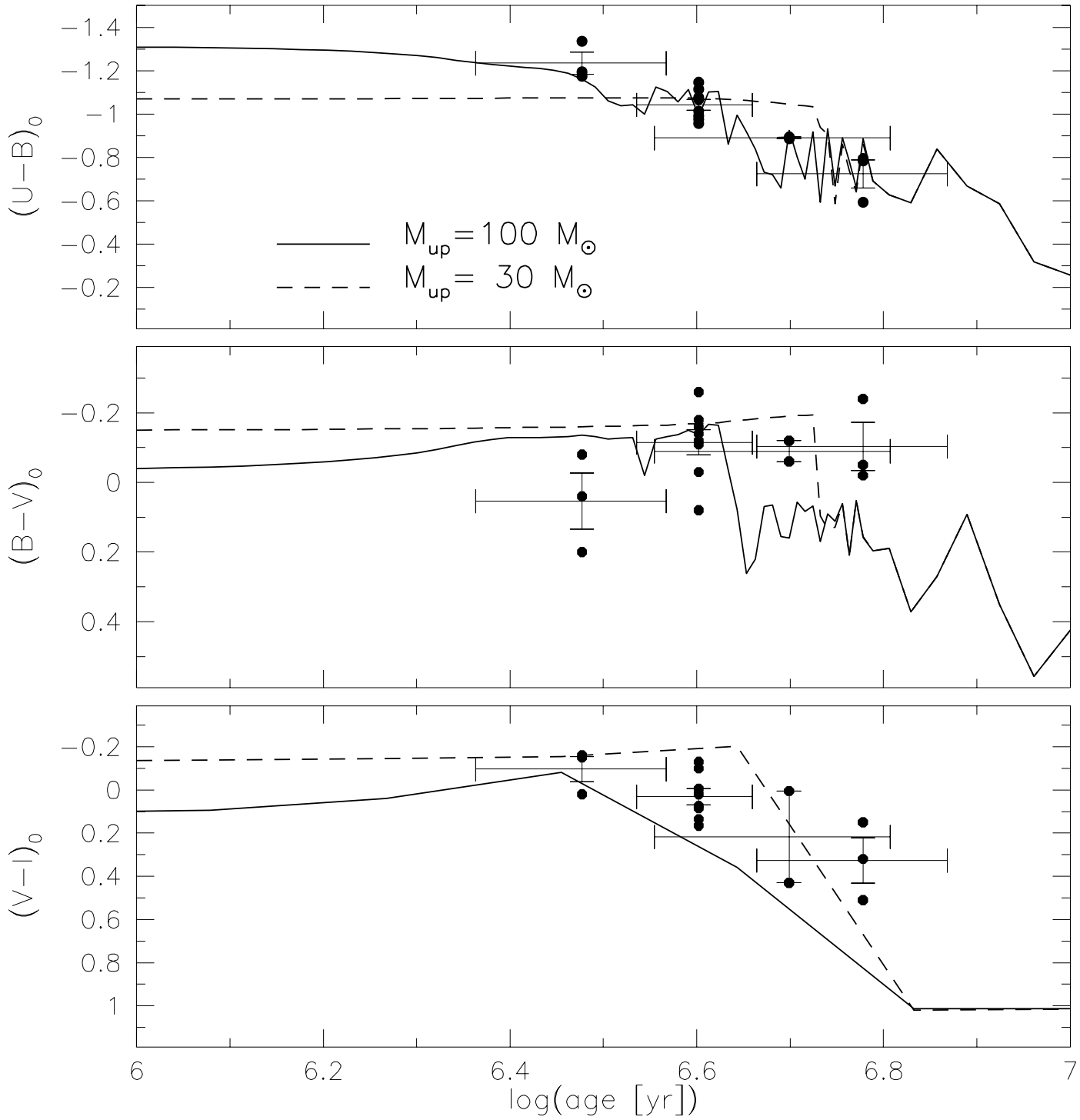

U−V ≦ −0.5
slope = 0.58 ±0.06
INCOMPLETE
log(N)
V
0
1
2
3
4
20
21
22
23
24
25
26

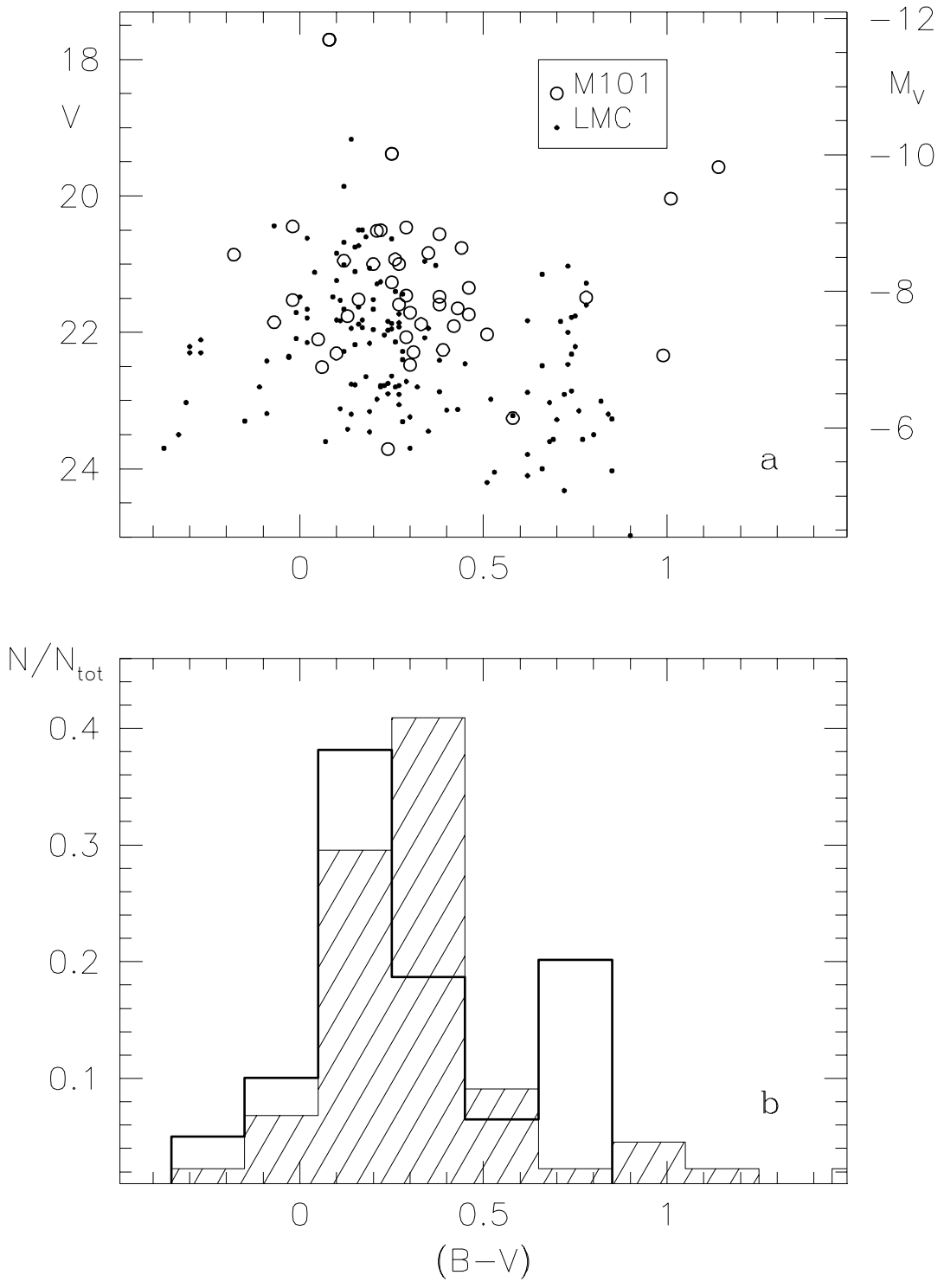

N
All OB associations and all HII regions
40
30
20
10
<E(B−V)> = 0.21 (Q parameter)
<E(B−V)> = 0.39 (Balmer ratio)
HII regions and corresponding OB associations only
8
6
4
2
0
0.2
0.4
0.6
0.8
1
E(B−V)

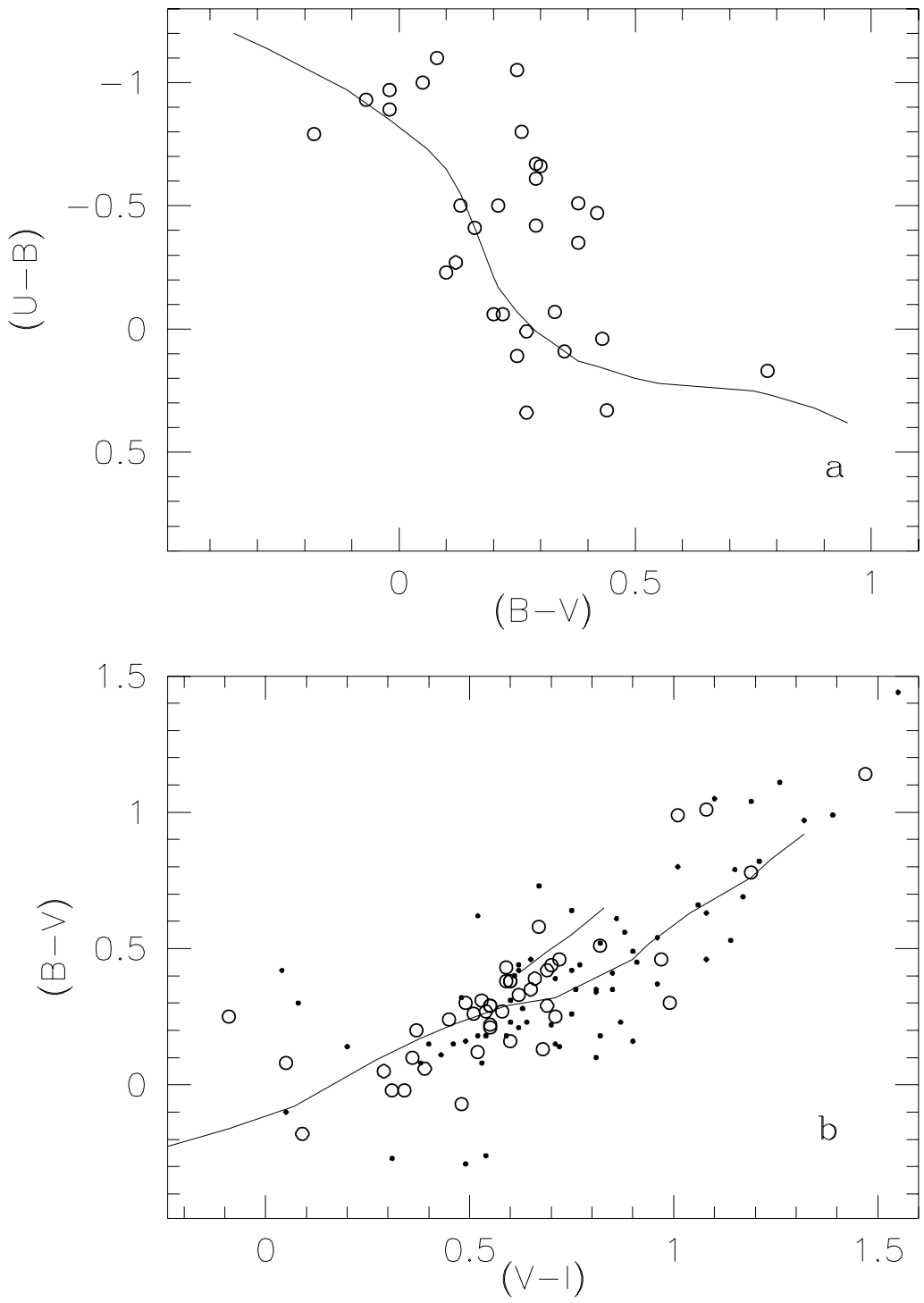

V_0
18
20
22
24
26
85 $M_\odot$
120 $M_\odot$
60 $M_\odot$
40 $M_\odot$
25 $M_\odot$
15 $M_\odot$
0
1
$(B-V)_0$

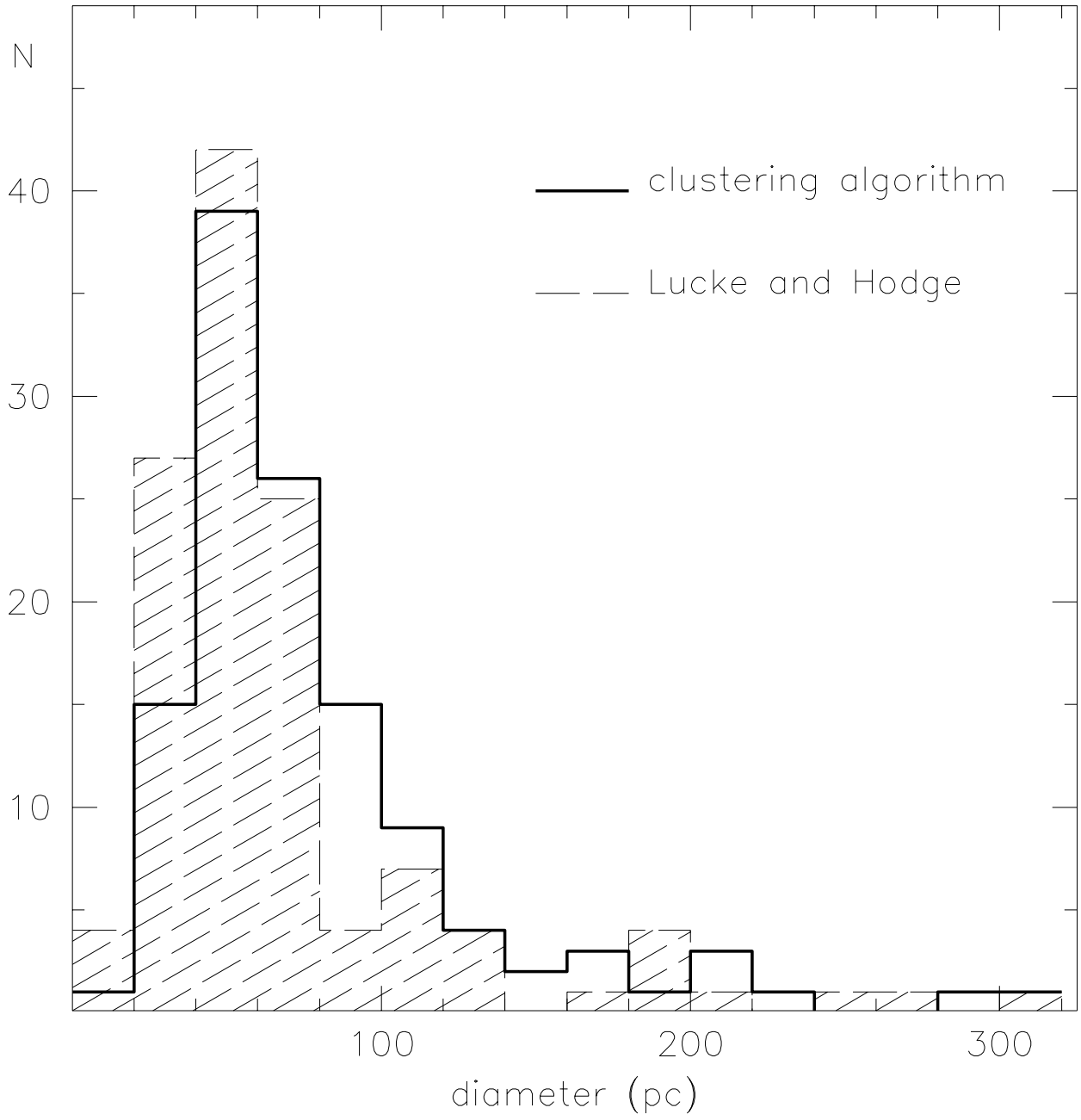

−1.2
−0.8
−0.4
0
0.4
0.8
(U−B)
−0.8
−0.4
0
0.4
0.8
(B−V)
U−V = −0.9
U−V = −0.4
V
I

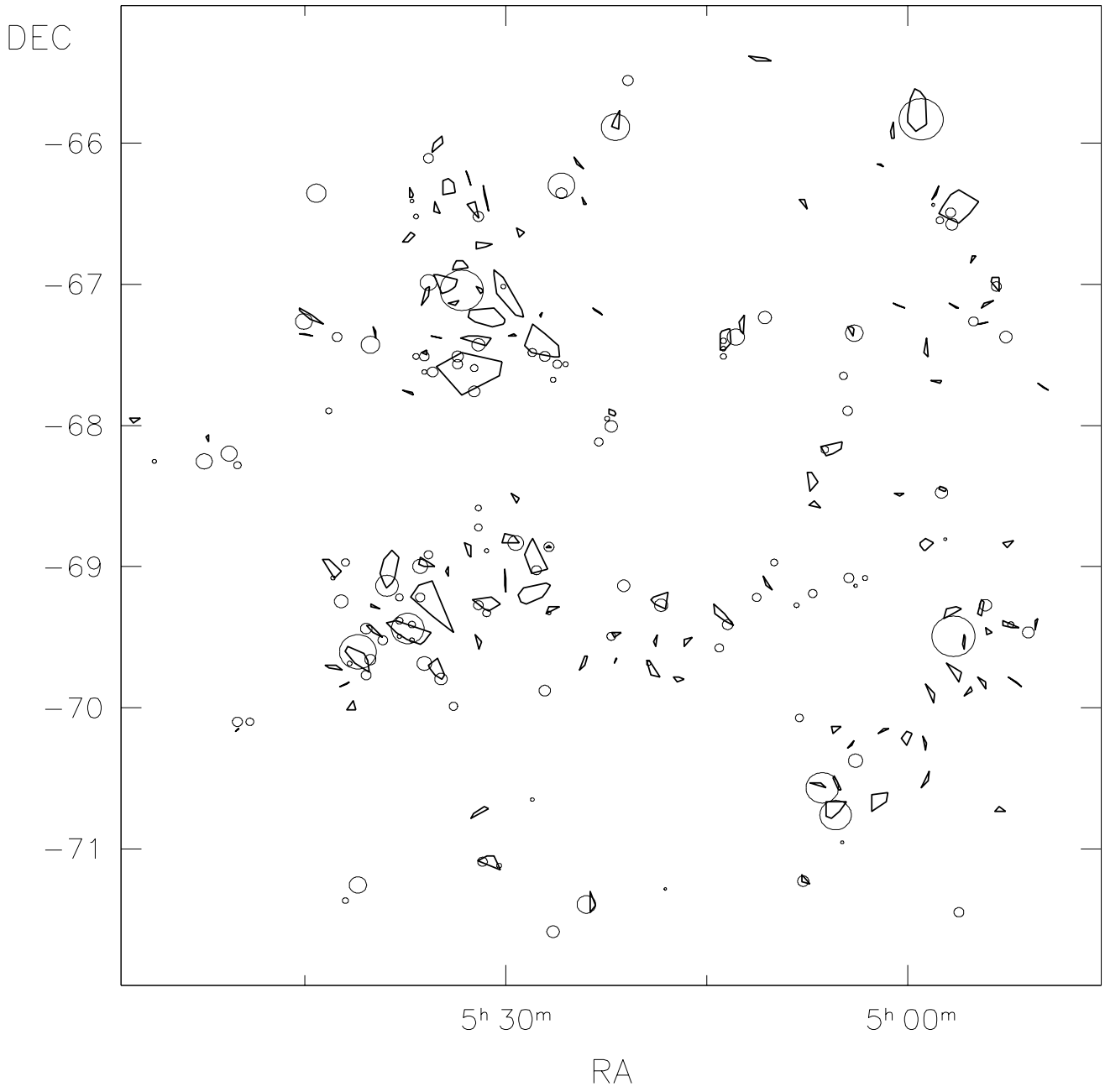

V
20
22
24
26
0
B−V
1
N(OB stars)
100
80
60
40
20
D (pc)
300
250
200
150
100
50
log Q_0
52
51
50
4
6
8
10
12
14
Age (Myr)


(U−B)0
(B−V)0
(V−I)0
−1.4
−1.2
−1
−0.8
−0.6
−0.4
−0.2
0
0.2
0.4
0.6
0.8
1
6
6.2
6.4
6.6
6.8
7
log(age [yr])
Mup=100 M⊙
Mup= 30 M⊙


M101
LMC
V
M_V
18
20
22
24
−12
−10
−8
−6
0
0.5
1
a
N/N_{tot}
0.4
0.3
0.2
0.1
b
(B−V)


−1
−0.5
0
0.5
(U−B)
0
0.5
1
(B−V)
a
1.5
1
0.5
0
(B−V)
0
0.5
1
1.5
(V−I)
b


N
40
30
20
10
clustering algorithm
Lucke and Hodge
100
200
300
diameter (pc)


DEC
−66
−67
−68
−69
−70
−71
5h 30m
5h 00m
RA